

Tension in the Void: Cosmic Rulers Strain Inhomogeneous Cosmologies

Miguel Zumalacárregui,^{a,c} Juan García-Bellido,^b Pilar Ruiz-Lapuente^a

^aInstitut de Ciències del Cosmos, Universitat de Barcelona IEEC-UB, Marti i Franques 1, E-08028 Barcelona, Spain

^bInstituto de Física Teórica UAM-CSIC, Universidad Autónoma de Madrid, Cantoblanco, 28049 Madrid, Spain

^cInstitute of Theoretical Astrophysics, University of Oslo, 0315 Oslo, Norway

E-mail: miguelzuma@icc.ub.edu, juan.garciabellido@uam.es, pilar@am.ub.es

Abstract. New constraints on inhomogeneous Lemaître-Tolman-Bondi (LTB) models alternative to Dark Energy are presented, focusing on adiabatic profiles with space-independent Big Bang and baryon fraction. The Baryon Acoustic Oscillation (BAO) scale at early times is computed in terms of the asymptotic value and then projected to different redshifts by following the geodesics of the background metric. Additionally, a model-independent method to constraint the local expansion rate using a prior on supernovae luminosity is presented. Cosmologies described by an adiabatic GBH matter profile with $\Omega_{\text{out}} = 1$ and $\Omega_{\text{out}} \leq 1$ are investigated using a Markov Chain Monte Carlo analysis including the latest BAO data from the WiggleZ collaboration and the local expansion rate from the Hubble Space Telescope, together with Union-II type Ia supernovae data and the position and height of the Cosmic Microwave Background acoustic peaks. The addition of BAO data at higher redshifts increases considerably their constraining power and represents a new drawback for this type of models, yielding a value of the local density parameter $\Omega_{\text{in}} \gtrsim 0.2$ which is 3σ apart from the value $\Omega_{\text{in}} \lesssim 0.15$ found using supernovae. The situation does not improve if the asymptotic flatness assumption is dropped, and a Bayesian analysis shows that constrained GBH models are ruled out at high confidence. We emphasize that these are purely geometric probes, that only recently have become sufficiently constraining to independently rule out the whole class of adiabatic LTB models.

Keywords: dark energy experiments; dark energy theory; baryon acoustic oscillations

ArXiv ePrint: [1201.2790](https://arxiv.org/abs/1201.2790)

Contents

1	Introduction	1
2	Lemaître-Tolman-Bondi Models	3
2.1	The constrained (adiabatic) GBH model	6
3	The Baryon Acoustic Scale in LTB universes	7
3.1	Free-falling scales in the LTB metric	9
3.1.1	BAO scale evolution beyond zero order	10
3.2	The physical BAO scale at early times and on the lightcone	10
3.3	Comparison with the observed BAO scale	11
3.3.1	The Alcock-Paczynski effect in LTB models	13
4	Observational Data	14
4.1	Type Ia Supernovae	14
4.2	Local Expansion Rate	15
4.3	Baryon Acoustic Scale	16
4.4	Cosmic Microwave Background	18
5	Analysis and Results	20
5.1	Homogeneous models	20
5.2	Inhomogeneous models	23
5.3	Model comparison	27
6	Discussion	29

1 Introduction

Recent years have witnessed enormous advance in the quantitative understanding of cosmology and the establishment of a Standard Cosmological Model. Its construction is grounded on the general relativistic description of space-time with the usual Einstein equations. The Ansatz for the space-time is a spatially homogeneous and isotropic Friedmann-Robertson-Walker (FRW) metric, chosen to satisfy the generalized Copernican Principle, or Cosmological Principle. In addition to the known particles (baryons, photons and neutrinos), two mysterious elements need to be added in order to account for all the observations. These give the name to the standard, Λ CDM model: Cold Dark Matter (CDM) plus a cosmological constant (Λ), the last one necessary to explain the dimming of distant supernovae [1, 2]. With the standard choice of the metric, the supernovae data imply that the universe is currently undergoing a phase of accelerated expansion.

The situation changes when the Cosmological Principle Hypothesis is dropped. As the supernovae we observe occur in our past lightcone, the changes in luminosity we interpret as time evolution might be due to spatial variations if the universe is not homogeneous. If the inhomogeneity represents an underdensity with a size comparable to the Hubble radius and our galaxy is located near its center, supernovae observations can be successfully accounted for without the introduction of new physics. This type of so-called “large void

models” can be described by a spherically symmetric Lemaître-Tolman-Bondi (LTB) metric, and have been studied as an alternative to the standard Λ CDM scenario [3–20]. Many different aspects of these alternative models have been considered over the past years, including observational constraints [21–38], the growth of perturbations [39–44], and the physics of the Cosmic Microwave Background (CMB) [45–55]. See reference [56] for a recent review.

If the time to Big Bang and the baryon-matter ratio are independent of the location, the LTB type of metric represents the gravitational growth of an adiabatic perturbation from an initially quasi-homogeneous state [39]. Although a Gigaparsec-sized void is difficult to reconcile with the standard inflationary paradigm, it might still be possible through large non-perturbative inhomogeneities associated with the stochastic nature of the inflaton evolution [57]. The only philosophical problem associated with this type of models is the requirement of being located very close to the center in order to preserve the great degree of isotropy observed in the CMB [46], but ultimately, only cosmological observations can tell us on the geometry and distribution of the cosmos and our position in it, provided that this question is meaningful.

The aim of this work is to analyze LTB models in the light of the most recent cosmological data. The Hubble Space Telescope has made a precise measurement of the local expansion rate [58] that challenges this type of void models, which typically require a low value to fit the CMB power spectrum [28, 29]. The determination of the Hubble parameter relies on the calibration of distant supernovae using Cepheid variable stars and the subsequent fit to a fiducial Λ CDM model in the low redshift range. Although applying priors directly on H_0 is fine for homogeneous cosmologies, LTB universes can have a very different evolution in the relevant redshift range. Therefore, our analysis is based on the intrinsic Ia supernova luminosity instead of the value of the Hubble parameter.

Further restrictions on this model are obtained from the scale of Baryon Acoustic Oscillations (BAO) and its evolution in an inhomogeneous cosmology by including the most recent BAO data up to redshift $z = 0.8$ provided by the WiggleZ collaboration [59] and Carnero *et al.* [60]. In a FRW cosmology, the BAO scale is space-independent and the constraints it yields arise from providing an independent measurement of cosmic distances relative to a *standard ruler*, with an initial length determined by the physics of the early universe. Once baryons decouple, the dominant effect on the observed physical scale is to be stretched by the expansion of the universe. However, in the less symmetric LTB cosmology the initially constant BAO scale grows differently: the physical scale acquires an additional radial dependence and is stretched differently in the longitudinal and transverse direction, due to the different expansion rates.

Adding information about the BAO scale at higher redshift reduces considerably the room for its value in the early universe. If the depth of the void is chosen to fit the supernovae luminosity distances, the inhomogeneous expansion produces a mismatch between the BAO scale at low and high redshift, posing a new problem for these models. Adding information on the CMB increases the discrepancies by restricting the initial acoustic scale, but the constraints are independent of the particular values, i.e, depend only on the *geometric* properties of the model regardless of the calibration of the standard rulers and candles. In particular, these constraints are independent of the primordial power spectrum, a critical assumption necessary to rule out large void models using the tension between the CMB and the local expansion rate [31] and are therefore complementary to these.

In section 2 we describe the general LTB void models, giving the corresponding Einstein-Friedmann equations, as well as the standard solution in absence of pressure. In a subsection

we describe the adiabatic assumption, i.e. that the time since Big Bang is space independent, and thus the model only depends on a single function, the inhomogeneous matter profile $\Omega_M(r)$. This is chosen to have the the GBH parameterization, presented in a subsection. In section 3 we study in detail the evolution of baryonic features in terms of free-falling trajectories of the background metric and compute the BAO observables. In section 4 we describe the cosmological data used to analyze the model, including a method to use the supernova luminosity to constrain the local expansion rate. In section 5 we analyze the results from the comparison of the model and the data and describe the tensions between the different datasets, as well as the result of different model comparison criteria. Finally, in section 6 we give our conclusions, discussing the generality of the results and stating several modifications that might render the model viable.

2 Lemaître-Tolman-Bondi Models

The LTB model describes general spherically symmetric space-times and can be used as a toy model for describing voids in the universe [61–63]. The starting point is the general metric

$$ds^2 = -dt^2 + X^2(r, t) dr^2 + A^2(r, t) d\Omega^2, \quad (2.1)$$

where $d\Omega^2 = d\theta^2 + \sin^2\theta d\phi^2$. Units in which $c = 1$ will be assumed in the following. Assuming a spherically symmetric matter source with negligible pressure, $T^\mu_\nu = -\rho_M(r, t) \delta^\mu_0 \delta^0_\nu$, the $(0, r)$ component of the Einstein equations, $G^t_r = 0$, sets the form of $X(r, t)$. The resulting cosmological metric becomes

$$ds^2 = -dt^2 + \frac{A'^2(r, t)}{1 - k(r)} dr^2 + A^2(r, t) d\Omega^2, \quad (2.2)$$

with an arbitrary function $k(r)$ playing the role of the spatial curvature parameter. The other components of the Einstein equations read [9, 21, 23]

$$H_T^2 + 2H_T H_R + \frac{k(r)}{A^2} + \frac{k'(r)}{AA'} = 8\pi G \rho_M, \quad (2.3)$$

$$2\dot{H}_T + 3H_T^2 + \frac{k(r)}{A^2} = 0, \quad (2.4)$$

where dots and primes denote ∂_t and ∂_r respectively, and we have defined the transverse (i.e. in the angular direction) and radial Hubble rates as

$$H_T \equiv \dot{A}/A, \quad \text{and} \quad H_R \equiv \dot{A}'/A'. \quad (2.5)$$

The reduced Hubble rate can be defined as usual: $H_{R/T} \equiv 100h_{R/T} \text{Km/Mpc/s}$. It is also useful to consider the normalized *shear*

$$\varepsilon \equiv \frac{H_T - H_R}{H_R + 2H_T}, \quad (2.6)$$

i.e. the difference between the radial and transverse expansion weighted by the total expansion [24]. This variable provides a local quantification of the departures with respect to homogeneous cosmologies, e.g. to characterize the growth of structure [43].

Integrating (2.3) yields

$$H_T^2 = \frac{F(r)}{A^3} - \frac{k(r)}{A^2}, \quad (2.7)$$

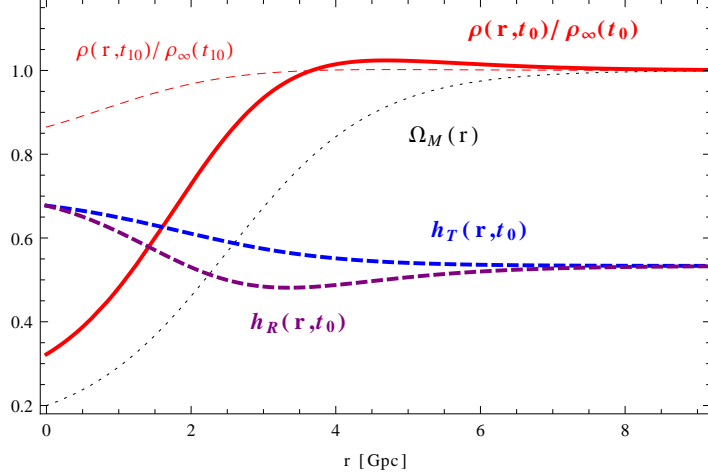


Figure 1. Physical parameters in the LTB model. The density contrast at $t(z = 0), t(z = 10)$ (red) shows the evolution from an initially less inhomogeneous state, and differs from the function $\Omega_M(r)$ (black dotted). The expansion rates in the radial (purple dashed) and transverse (blue dashed) directions differ the most where the void is steeper. The profile shown has $R = 2.5, \Delta R = 1$.

in terms of another arbitrary function $F(r)$. Substituting it into the first equation gives

$$\frac{F'(r)}{A'A^2(r, t)} = 8\pi G \rho_M(r, t), \quad (2.8)$$

where $\rho_M(r, t)$ is the physical matter density. Since $F(r)$ is time-independent, one can choose $t = t_0$ and compute the integrated matter density in a comoving volume today, $V = 4\pi r^3/3$, as $\bar{\rho}(r) = \frac{1}{V} \int_0^r 4\pi r'^2 dr' \rho_M(r', t_0)$, and construct with it the ratio $\Omega_M(r) \equiv \bar{\rho}(r)/\bar{\rho}_c(r)$, where $\bar{\rho}_c(r) = 3H_0^2(r)/8\pi G$ is the critical density in that volume [24].

The boundary condition functions $F(r)$ and $k(r)$ are specified by the nature of the inhomogeneities through the local Hubble rate, the integrated mass ratio and the local spatial curvature,

$$F(r) = H_0^2(r) \Omega_M(r) A_0^3(r) = 8\pi G \int_0^r dr' r'^2 \rho_M(r', t_0), \quad (2.9)$$

$$k(r) = H_0^2(r) (\Omega_M(r) - 1) A_0^2(r), \quad (2.10)$$

where functions with subscripts 0 correspond to present day values, $A_0(r) \equiv A(r, t_0)$ and $H_0(r) \equiv H_T(r, t_0)$. With these definitions, the (position dependent) transversal Hubble rate can be written as [9, 21]

$$H_T^2(r, t) = H_0^2(r) \left[\Omega_M(r) \left(\frac{A_0(r)}{A(r, t)} \right)^3 + (1 - \Omega_M(r)) \left(\frac{A_0(r)}{A(r, t)} \right)^2 \right], \quad (2.11)$$

and we fix the gauge by setting $A_0(r) = r$. For fixed r and $\Omega_M < 0$ the above expression is equivalent to the Friedmann equation, and has an exact parametric solution in terms of the

variable η :

$$A(r, t) = \frac{\Omega_M(r)}{2[1 - \Omega_M(r)]} [\cosh(\eta) - 1] A_0(r), \quad (2.12)$$

$$H_0(r)t = \frac{\Omega_M(r)}{2[1 - \Omega_M(r)]^{3/2}} [\sinh(\eta) - \eta]. \quad (2.13)$$

Very good approximate solutions can also be found by Taylor expanding around an Einstein de Sitter solution [23].

In addition to the solution of Einstein Equations (2.12,2.13) it is necessary to obtain the coordinates on the lightcone as a function of redshift. For light traveling along radial null geodesics, $ds^2 = d\Omega^2 = 0$ yields

$$\frac{dt}{dr} = \mp \frac{A'(r, t)}{\sqrt{1 - k(r)}}, \quad (2.14)$$

which, together with the redshift equation [21, 63],

$$\frac{d \log(1 + z)}{dr} = \pm \frac{\dot{A}'(r, t)}{\sqrt{1 - k(r)}}, \quad (2.15)$$

allows us to write a parametric set of differential equations, with $N = \log(1 + z)$ being the effective number of e-folds before the present time,

$$\frac{dt}{dN} = - \frac{A'(r, t)}{\dot{A}'(r, t)}, \quad (2.16)$$

$$\frac{dr}{dN} = \pm \frac{\sqrt{1 - k(r)}}{\dot{A}'(r, t)}, \quad (2.17)$$

where the equations are integrated with the initial condition $r(0) = 0$, $t(0)$ obtained from (2.12,2.13) for $r = 0$, $A = A_0$.

The angular diameter distance is given by the $d\Omega$ element of the metric evaluated on the lightcone, and is related to the luminosity distance by the redshift due to photon redshift and time dilation

$$D_A(z) = A(r(z), t(z)), \quad (2.18)$$

$$D_L(z) = (1 + z)^2 A(r(z), t(z)). \quad (2.19)$$

The dynamics of the LTB metric in the only-matter approximation discussed above are fully specified by the two functions $\Omega_M(r)$, $H_0(r)$ independently of the type of matter present, as long as it exerts no pressure. But by dropping the symmetries of the FRW model a spherically symmetric but inhomogeneous mixture of baryonic and dark matter can be accommodated. A possible parameterization in terms of the total matter density would be

$$f_b(r) \equiv \frac{\rho_b(r, t)}{\rho_m(r, t)}, \quad (2.20)$$

where there is no time dependence because the energy density of baryons and dark matter evolves identically at late times.

Before explaining the choice of matter profile and the physical restrictions on the model, let us briefly summarize the approximations used throughout this work

- Spherical symmetry as given by (2.2) and perfectly central location of our galaxy at $r = 0$, $t = t_0$ as initial conditions for the lightcone integration (2.16).
- Radiation energy and pressure neglected as a source of the expansion (2.11).
- Early time and large radius FRW limit of the model, necessary to compute the BAO scale (Section 3) and the relative locations of the CMB peaks (Section 4.4).
- Perturbations of the LTB metric neglected. The evolution of the BAO scale from early times is studied by analyzing the geodesics of the background metric (2.2) (Section 3).

2.1 The constrained (adiabatic) GBH model

General LTB models are uniquely specified by the two functions $k(r)$ and $F(r)$ or equivalently by $H_0(r)$ and $\Omega_M(r)$, but to test them against data it is necessary to parameterize the functions, so that a finite dimensional space is analyzed. In this paper we will use the GBH model [23] to describe the matter profile in terms of a reduced number of parameters. In addition to the choice for the free function $\Omega_M(r)$, we further impose that the time to Big Bang is space-independent

$$t_{\text{BB}}(r) = H_0(r)^{-1} \left(\frac{1}{\sqrt{\Omega_K(r)}} \sqrt{1 + \frac{\Omega_M(r)}{\Omega_K(r)}} - \frac{\Omega_M(r)}{\sqrt{\Omega_K^3(r)}} \sinh^{-1} \sqrt{\frac{\Omega_K(r)}{\Omega_M(r)}} \right) = t_0, \quad (2.21)$$

where $\Omega_K(r) = 1 - \Omega_M(r)$. The above expression can be obtained from integration of (2.11) [21, 23] or by solving for $A = A_0(r)$ in (2.12, 2.13). This condition reduces the functional freedom associated to $H_0(r)$ to a single normalization constant H_0 , that is related to the overall age of the universe.

Additionally, we require that there are no large scale baryonic isocurvature modes, i.e. the baryon fraction (2.20) is constant. This type of voids can be regarded as the gravitational collapse of a large scale, adiabatic and spherically symmetric perturbation which has a small amplitude at early times. Its adiabatic nature is related to the fact that there is only one functional degree of freedom that sets the shape of the remaining free functions ($\Omega_M(r)$ in our case, which in turn fixes $H_0(r)$ and the baryon fraction).

The above conditions give a relation between $H_0(r)$, $\Omega_M(r)$ and $f_b(r)$, and hence constrain the models to one free function. Our chosen model is thus given by

$$\Omega_M(r) = \Omega_{\text{out}} + (\Omega_{\text{in}} - \Omega_{\text{out}}) \left(\frac{1 - \tanh[(r - R)/2\Delta R]}{1 + \tanh[R/2\Delta R]} \right) \quad (2.22)$$

$$H_0(r) = H_0 \left[\frac{1}{\Omega_K(r)} - \frac{\Omega_M(r)}{\sqrt{\Omega_K^3(r)}} \sinh^{-1} \sqrt{\frac{\Omega_K(r)}{\Omega_M(r)}} \right] = H_0 \sum_{n=0}^{\infty} \frac{2[\Omega_K(r)]^n}{(2n+1)(2n+3)}, \quad (2.23)$$

$$f_b(r) = f_b = \text{constant} \quad (2.24)$$

where the second equation follows from (2.21), and the third by demanding constant baryon to matter ratio. This parameterization was introduced to lower the shear around the void wall (e.g. with respect to Gaussian profiles) and allow an unified description of cuspy and flat central regions [23]. Each void model is specified by the following parameters:

- Ω_{in} : Matter/curvature fraction at the center of the void (equations 2.8-2.10). As deeper voids produce more fictitious acceleration, this parameter plays a major role in the constraints presented in Section 5.
- Ω_{out} : Asymptotic ($r \rightarrow \infty$) matter/curvature fraction in which the inhomogeneous region is embedded. Two possibilities will be considered separately depending on the asymptotic curvature of the universe:
 - CGBH**: Flat $\Omega_{\text{out}} = 1$, as suggested by inflationary physics.
 - OCGBH**: Open $\Omega_{\text{out}} \leq 1$, which allows a better fit to the CMB.
- ΔR : Slope of the inhomogeneity. Smaller values of ΔR produce steeper profiles and increase the shear (2.6).
- R : Shape of the void. $\Delta R \ll R$ describes an inhomogeneity with a central plateau of approximately constant density, while $\Delta R \gg R$ produces a cuspy central region.
- H_0 : Expansion rate normalization that determines the Big Bang time (2.21).
- f_b : Baryon fraction over the total matter content. Its value affects the pre-recombination physics and determines the value of the BAO scale and CMB peak locations.

The choice of the constrained model is important because, in our gauge, void models with an *inhomogeneous* Big Bang would contain a mixture of growing and decaying modes, and consequently the void would not disappear at early times, making them incompatible with the Standard Big Bang scenario [39]. By restricting ourselves to adiabatic LTB models the central void is reduced to an insignificant perturbation in an otherwise homogeneous universe described by an FRW metric, both at large distances *and* early times. This requirement, together with the condition of constant baryon fraction, ensures the space-independence of the early BAO scale, which is a key part of the present analysis.

3 The Baryon Acoustic Scale in LTB universes

Inhomogeneous cosmologies stretch the BAO scale differently than their homogeneous cousins. There are three potential effects to be addressed when computing the BAO scale in LTB models at the background level:

1. Inhomogeneous expansion: The matter distribution will source the expansion of the universe in a position dependent way. Therefore, there will be a radial dependence of the physical scale in addition to the time dependence.
2. Anisotropic expansion: In general the expansion rate in the radial and transverse direction will be different $H_T \neq H_R$, resulting in two different BAO scales $l^T \neq l^R$, as seen by a central observer.¹
3. Radial coordinate drift: Displacements in the radial direction are not a symmetry of the LTB metric and the free-falling baryon features are not ensured to remain at constant r . In Section 3.1 we show that this effect does not occur for timelike geodesics.

¹The relation between this effect and the Alcock-Paczynski test will be discussed in Section 3.3.1.

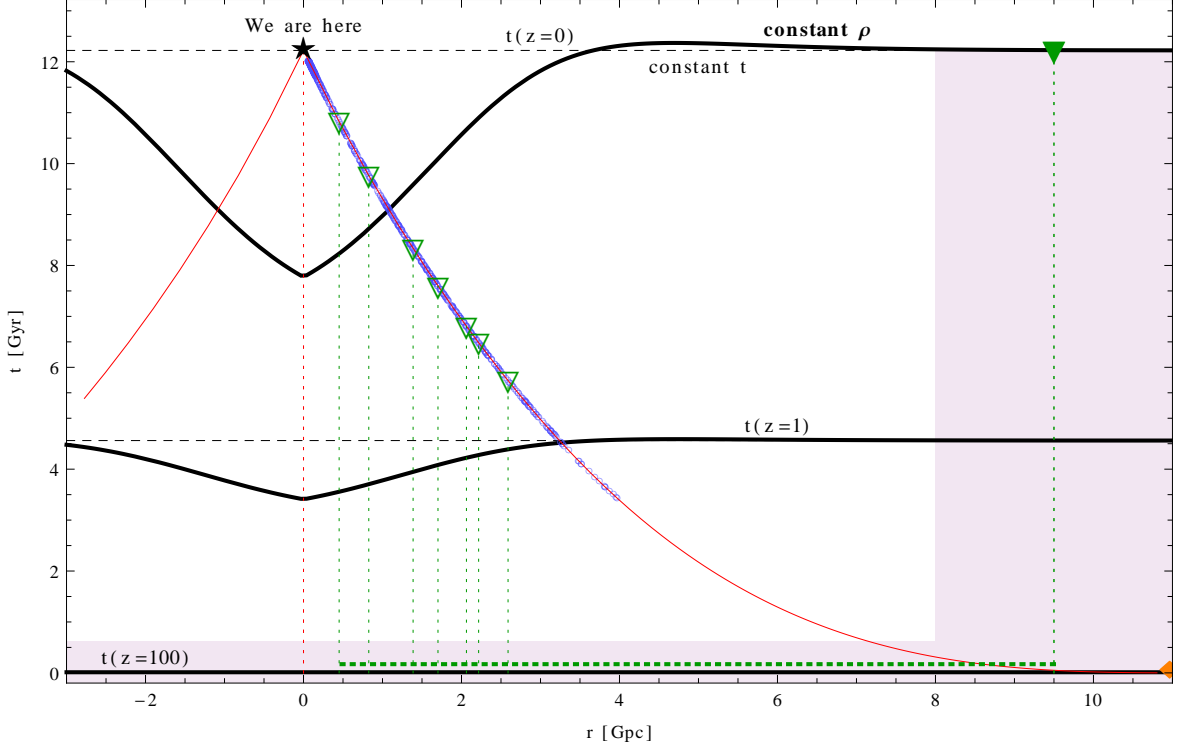


Figure 2. The LTB model with space-independent Big Bang. Black lines represent hypersurfaces of constant time $t = t(z)$ for $z = 0, 1, 100$ (dashed) and constant density $\rho(r, t) = \rho(r_\infty, t(z))$ (thick, continuous). The filled areas show schematically the regions in which the void can be considered homogeneous (early times and large radii). Red constant lines represent our lightcone, where the coordinates of SNe (blue circles on the left) and BAO (green triangles on the right) observations has been added. Vertical dotted lines correspond to the geodesic worldlines of our galaxy (red) and the BAO fiducial locations (green). The physical BAO scale at different z is obtained from the asymptotic value (represented by the filled green triangle), extrapolated to early times, for which the universe is approximately homogeneous (horizontal green dotted line) and evaluated at the lightcone coordinates using the LTB metric (see Section 3 for the details).

Possible effects from higher order corrections will be discussed at the end of Section 3.1.1.

Our approach to predict the BAO scale in LTB models with space-independent Big Bang time relies on the homogeneity properties of the metric at large radius (i.e. the profile flattens) and early times (i.e. the Big Bang time and the baryon fraction are independent of the position). Relaxing this assumptions would require a more careful treatment which goes beyond the scope of this work. We first analyze the evolution of the BAO scale in the inhomogeneous cosmology by following the geodesics of the LTB metric (Section 3.1). Afterwards, the asymptotic physical scale computed in the limit $r \gg R$, ΔR using the fitting formulae is extrapolated to a suitable early time t_e at which the void is just a negligible perturbation. The obtained value can be then projected to the coordinates of observation $r(z), t(z)$ using the previous results (Section 3.2). Finally, the physical scale is related to the observed quantity d_z quoted by the galaxy surveys (Section 3.3). The procedure is sketched in Figure 2.

The derivation we are presenting avoids using certain concepts that might be equivocal when used for inhomogeneous cosmologies. In particular, we will only use redshift as a coordinate on the lightcone or in the asymptotic region when the FRW limit can be applied. We will also avoid the term “comoving” and will refer to “coordinate” instead, as well as pay special attention to distinguishing physical distances and relative coordinate separations.

3.1 Free-falling scales in the LTB metric

The propagation of sound waves in the baryon-photon fluid present in the early, expanding, universe leaves an imprint at a characteristic length that will be observable in the late universe as a peak in the correlation function of galaxies [64, 65]. When the universe becomes neutral, baryon-photon interactions render effectively zero and the baryonic overdensities start behaving as free-falling test bodies. We can therefore analyze the relative separation of the initial baryon clumps and the galaxies they will form by following the geodesics of the LTB metric: $x^\mu(\tau) = \{t(\tau), r(\tau), \theta(\tau), \phi(\tau)\}$, where $\dot{x}^\mu = \frac{dx^\mu}{d\tau}$. The BAO scale can be traced simply by following two nearby trajectories with an initial separation equal to the baryon acoustic scale at a sufficiently early time.

The transverse evolution is the simplest. Since rotations are an isometry of the LTB metric, the momentum in the angular directions is conserved and trajectories with $\dot{\phi}, \dot{\theta} = 0$ initially will remain at constant angular coordinates. This can be readily seen from the geodesic equation for the θ coordinate

$$\ddot{\theta} + 2\frac{A'}{A}\dot{r}\dot{\theta} + 2\frac{\dot{A}}{A}\dot{t}\dot{\theta} = 0, \quad (3.1)$$

for which $\theta(\tau) = \theta_0$ is a solution. Its stability follows by demanding timelike, slow geodesics for which $\dot{t} \gg \dot{r}$ and noting that the second term is positive in an expanding universe ($\dot{A} > 0$, $H_T > 0$) and acts as a friction against the angular velocity $\dot{\theta}$. Therefore, initial angular separation $\Delta\theta$ is conserved in coordinate space and the associated, transverse physical scale can be obtained integrating the angular element of the metric $l_{\text{phys}}^T = A(r, t)\Delta\theta$.

Since shifts in the radial direction are not an isometry of the LTB metric, \dot{r} is not automatically conserved and the determination of the radial acoustic scale requires a more careful treatment. The geodesic equations for a trajectory with $\dot{\phi}, \dot{\theta} = 0$ are

$$\ddot{t} + \frac{A'\dot{A}}{1-k(r)}\dot{r}^2 = 0, \quad (3.2)$$

$$\ddot{r} + \left[\frac{k'(r)}{2(1-k(r))} + \frac{A''}{A'} \right] \dot{r}^2 + 2\frac{\dot{A}}{A'}\dot{t}\dot{r} = 0. \quad (3.3)$$

Similarly to the angular case, a particle initially at rest at some early time t_e , $\dot{r}(t_e) = 0$, will remain at constant radial coordinate location $r(\tau) = r(t_e)$. Timelike trajectories with $\dot{t} \gg \dot{r}$ are again stable in an expanding universe due to the longitudinal Hubble friction term $\dot{A}/A' > 0$, and geodesics will remain at constant coordinate separations at different cosmic epochs.² The physical distance in the r direction can be obtained simply by integration using the radial element of the metric $l_{\text{phys}}^R = \int \sqrt{g_{rr}} dr \approx A'/\sqrt{1-k}\Delta r$.

²The situation would considerably change if Γ_{tt}^r was different from zero in the LTB metric. It might be as well possible to devise profiles for which the first term in (3.3) overcomes the second for sufficiently rapid geodesics, i.e. high \dot{r}/\dot{t} , but this is not the case for the models under study.

To summarize, since coordinate locations are conserved in geodesic evolution, we can provide the following relation for freely falling, physical scales in the LTB metric at different times t, t_e in the transverse and longitudinal directions

$$l_{\text{phys}}^T(r, t) = \frac{A(r, t)}{A(r, t_e)} l_{\text{phys}}^T(r, t_e), \quad (3.4)$$

$$l_{\text{phys}}^R(r, t) = \frac{A'(r, t)}{A'(r, t_e)} l_{\text{phys}}^R(r, t_e). \quad (3.5)$$

3.1.1 BAO scale evolution beyond zero order

The above analysis so far has dealt with the differences between homogeneous and inhomogeneous models at the zero order level. In a FRW universe, the BAO scale is constant in coordinate space also in first order perturbation theory. This is due to the lack of scale dependence of sub horizon perturbations at late times $\delta_k(t) = D(t)\delta_k(t_0)$ [66], which preserves the shape of the power spectrum and the two point correlation function (both are related by a Fourier transform). The first corrections come through nonlinear effects, which act reducing the BAO scale at the few percent level, due to the attraction between the initial perturbation and the baryon clumps at the characteristic length [67, 68]. These effects will eventually become relevant as the precision of surveys and the reconstruction techniques improve.

In inhomogeneous universes the situation is different, since the lack of symmetry produces the failure of the perturbation decomposition and the treatment of scalar perturbations (in the metric and matter density) have to be considered together with vector and tensor perturbations [39, 40]. The vorticity (vector) component is subdominant because the LTB metric is rotationally invariant, but the scalar potential is sourced at linear order by a term proportional to the background shear traced with the tensor perturbations. Fortunately, for the GBH profiles considered here, the background shear is below 5% and these contributions will be subdominant with respect to the much larger effect of the inhomogeneous expansion (see Figure 3 and Section 3.3). February *et al.* recently presented the numerical computation of the BAO scale in LTB models within linear theory, and considering only scalar perturbations [44]. They found a shift on the BAO scale at the percent level, which is nevertheless considerably smaller than the departures induced by the inhomogeneous and anisotropic expansion discussed above.

Further support for the assumption of a constant BAO scale in coordinate space is provided by N-body numerical studies. Alonso *et al.* run simulations in which inhomogeneous matter profiles are implemented through an initial underdensity of Gpc size. Their results show that the (local) matter density contrast grows with the scale factor in a way analogous to that of an open universe with a value of the matter density $\Omega_M(r)$ corresponding to the appropriate location r [41], showing an effective decoupling between the small scale clustering and the evolution of the void. Corrections from the large scale inhomogeneity are proportional to the local shear weighted by a factor $\mathcal{O}(1)$ [43], and are hence small for the profiles allowed by observations.

3.2 The physical BAO scale at early times and on the lightcone

The solutions of the LTB metric with space-independent Big Bang represent an inhomogeneity that grows due to gravitaional instability out of a very homogeneous state. For typical voids at $t(z = 100)$ the physical density contrast $\rho_m(r, t)/\rho_m(r_\infty, t)$ is of order 1%, while at $t(z = 1000)$ it shrinks to $\sim 0.1\%$. As the baryonic features develop between $t \sim 0$ and

$t \sim t(z = 1000)$, it is a good approximation to consider that the physics responsible for recombination and the origin of the baryon acoustic scale are indistinguishable from their counterparts in homogeneous cosmologies. It will be therefore assumed that for models with space-independent Big Bang the physical BAO scale is isotropic and coordinate independent at early times on constant time hypersurfaces.³

$$l_{BAO}(r(z), t_e) \approx l_{BAO}(r_\infty, t_e). \quad (3.6)$$

The early time BAO scale can be obtained from the asymptotic value at different times using equation (3.4) or (3.5). In the $r \rightarrow \infty$ limit the universe is indistinguishable from a FRW cosmology, and we can compute the BAO scale using the fitting formulae provided by Eisenstein and Hu [64] in terms of the asymptotic values of the matter density and baryon fraction. These effective values are obtained by projecting the LTB parameters on the lightcone at a very high redshift $z_e \approx 100$, for which 1) $H_T \approx H_R$ and the universe is approximately homogeneous on a constant $t = t(z_e)$ hypersurface, 2) the point $r(z_e)$ is away from the inhomogeneous region and 3) the radiation contribution is still negligible. These values are given by

$$\Omega_m^{\text{eff}} = \frac{\rho(r_\infty, t_0)}{3H_T^2(r_\infty)} \approx \Omega_{\text{out}}, \quad (3.7)$$

$$\Omega_b^{\text{eff}} \approx f_b \Omega_{\text{out}}, \quad (3.8)$$

$$H_0^{\text{eff}} = \frac{2H_T(z_e) + H_R(z_e)}{3\sqrt{\Omega_m^{\text{eff}}(1+z_e)^3 + (1-\Omega_m^{\text{eff}})(1+z_e)^2}}. \quad (3.9)$$

Here H_0^{eff} can be understood as “rewinding” the LTB value of the average expansion rate $2H_T(z_e)/3 + H_R(z_e)/3$ using the FRW asymptotic value of Ω_m .

The fitting formulae give a comoving scale in a FRW universe which coincides with the physical value at $t = t_0$ for the usual definition of the scale factor in the asymptotic FRW metric $a(t_0) = a_0 = 1$. The corresponding scale at t_0 is valid in the limit $r \rightarrow \infty$, but can be related to the radial and transverse physical scales using (3.4,3.5,3.6). For a point located on the past lightcone of the central observer, the values are

$$l_{BAO}^T(z) \equiv \xi_T(z) l_{BAO}(r_\infty, t_0) = \frac{A(r(z), t(z))}{A(r(z), t_e)} \frac{A(r_\infty, t_e)}{A(r_\infty, t_0)} l_{BAO}(r_\infty, t_0), \quad (3.10)$$

$$l_{BAO}^R(z) \equiv \xi_R(z) l_{BAO}(r_\infty, t_0) = \frac{A'(r(z), t(z))}{A'(r(z), t_e)} \frac{A'(r_\infty, t_e)}{A'(r_\infty, t_0)} l_{BAO}(r_\infty, t_0). \quad (3.11)$$

The first equalities define a transversal and longitudinal rescaling factors (see Figure 3), which reduce to $(1+z)^{-1}$ in the homogeneous limit.

3.3 Comparison with the observed BAO scale

The BAO scale can be extracted from the galaxy correlation function measured in galaxy surveys. What is actually observed is a combination of the angular correlation θ_{BAO} and the

³A more physical criterion would be to consider constant density hypersurfaces. Although the difference is of order 0.1% in models with space-independent Big Bang, it might render helpful to generalize the treatment of BAO for profiles with general $H_0(r)$.

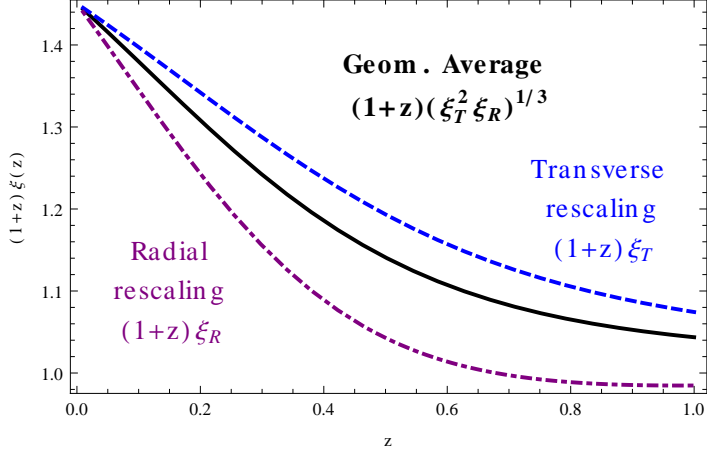


Figure 3. Effects on the LTB metric on the BAO scale with respect to their FRW analogues. The difference between the transverse (blue, dashed) and longitudinal (purple, dot-dashed) factors accounts for the anisotropy of the scales in the angular and transverse direction, respectively. The geometric averaged rescaling factor (black solid) is used for volumetric BAO determinations through the quantity $d_z^{\text{LTB}} = (1+z)\xi(z)d_z^{\text{FRW}}$ (3.19). Note that all three curves coincide in $r = 0$, since the void is locally isotropic at the center.

correlation in redshift space Δz_{BAO} [69]. In order to compare the models with observations, we need to relate the isotropized correlation measured by the surveys

$$d_z = \left(\theta_{\text{BAO}}^2 \frac{\Delta z_{\text{BAO}}}{z} \right)^{1/3}, \quad (3.12)$$

to the physical scales computed in the previous section.⁴

The angular correlation can be readily obtained from the definition of the angular diameter distance as the ratio between a known (transverse) length and the angle it subtends

$$\theta_{\text{BAO}} = \frac{l_{\text{BAO}}^T(z)}{D_A(z)}. \quad (3.13)$$

The redshift correlation can be related to the radial coordinate separation by means of the redshift equation (2.15)

$$\Delta z_{\text{BAO}} = \int \frac{dz}{dr} dr \approx \frac{(1+z)\dot{A}'(r(z), t(z))}{\sqrt{1-k(r)}} \Delta r_{\text{BAO}}, \quad (3.14)$$

where in the second equality the integrand has been assumed to be constant. Similarly, the coordinate characteristic scale Δr is given in terms of the physical scale through an integral

$$\Delta r_{\text{BAO}} \approx \frac{\sqrt{1-k(r)}}{A'(r(z), t(z))} l_{\text{BAO}}^R(z). \quad (3.15)$$

⁴This section follows section 4.6.3 of Biswas et al. [29]. Our result (3.17) has the same form as their equation (4.48) after several coefficients cancel out. However, their computation assumes the BAO scale to be given by the local values of $\Omega_M(r), \Omega_B(r), H_0(r)$ instead of obtaining them from the asymptotic FRW value and the factor $(1+z_{\text{rec}})$ is taken to be given by the volume element comparison on the worldline of constant $r = r(z)$ instead of by the asymptotic value $r \rightarrow \infty$.

Both equations relate the physical correlation with the redshift correlation

$$\Delta z_{BAO} = (1+z)H_R(z)l_{BAO}^R(z) \quad (3.16)$$

Constructing the geometric mean (3.12) using (3.13,3.16) is straightforward:

$$d_z^{LTB} = \left(\frac{H_R}{z}(1+z)\frac{1}{D_A(z)^2} \right)^{1/3} \xi(z) l(r_\infty, t_0), \quad (3.17)$$

where the scale conversion arising from (3.10,3.11) has been introduced in the factor $\xi(z) \equiv (\xi_R(z)\xi_T^2(z))^{1/3}$, given by

$$\xi(z) = \left(\frac{A'(r(z), t(z))}{A'(r(z), t_e)} \frac{A'(r_\infty, t_e)}{A'(r_\infty, t_0)} \right)^{1/3} \left(\frac{A(r(z), t(z))}{A(r(z), t_e)} \frac{A(r_\infty, t_e)}{A(r_\infty, t)} \right)^{2/3}, \quad (3.18)$$

using a suitable early time $t_e = t(z \sim 100)$ to convert the scale as described in the previous section. Note that due to the FRW limit, the ratios of the factors computed at r_∞ can be expressed as redshift factors $a(t_e)/a_0 = (1+z_e)^{-1}$.

Equation (3.17) can be easily related to the usual expression for d_z

$$d_z^{LTB} = (1+z)\xi(z)\frac{l(r_\infty, t_0)}{D_V(z)} = (1+z)\xi(z)d_z^{\text{FRW}}. \quad (3.19)$$

in terms of the usual volume distance

$$D_V(z) = \left((1+z)^2 D_A(z)^2 \frac{z}{H_R(z)} \right)^{1/3}. \quad (3.20)$$

Relation (3.19) absorbs the effects of the inhomogeneous rescaling in the BAO observations, which pick up a factor $(1+z)\xi(z)$ with respect to the FRW case. The difference between the two rescaling factors accounts for the anisotropy between the transverse and longitudinal BAO scales, while their redshift dependence is a consequence of the inhomogeneity. Both effects are shown in Figure 3. Note also that there will be an additional difference because of the modified relations between the angular diameter distance (related to the transverse expansion) and the longitudinal expansion rate entering the geometric mean distance (3.20).

3.3.1 The Alcock-Paczynski effect in LTB models

The Alcock-Paczynski (AP) effect [70] is the geometric distortion of spherical objects due to cosmological expansion, since distances in the radial direction away from an observer are determined in redshift space, while transverse distances are seen as angular separations in the sky. This motivates the definition of the dimensionless *distortion factor*:

$$f_{\text{FRW}}^{\text{AP}}(z) \equiv \frac{\Delta z}{\Delta \theta} = D_A(z)H_R(z)(1+z). \quad (3.21)$$

In a homogeneous universe, the above relation can be tested against spherical (or spherically distributed) objects for which Δz and $\Delta \theta$ are measured.⁵ This technique has been used to constrain cosmological models [71–73].

⁵In practice, the AP test is difficult to perform due to dynamical effects such as the redshift space distortions caused by cosmic structures, which induce peculiar velocities that affect the redshift in a systematic way.

In LTB models with space-independent Big Bang time, initially spherical distributions are intrinsically distorted due to the local shear, as discussed in Section 3.1. Using the angular and redshift projection of physical distances for the inhomogeneous models given by equations (3.13, 3.16), the analogue of the AP relation is modified by the ratio of the radial and transverse rescaling factors

$$f_{\text{LTB}}^{\text{AP}}(z) = \frac{\xi_R(z)}{\xi_T(z)} D_A(z) H_R(z) (1+z) = \frac{\xi_R(z)}{\xi_T(z)} f_{\text{FRW}}^{\text{AP}}(z). \quad (3.22)$$

The values of these factors in both directions can be seen in Figure 3. As the universe expands faster in the transverse than in the radial direction, the distortion factor has a lower value than in FRW models, on top of the different relation between $D_A(z)$ and $H_R(z)$.

The distortion factor (3.22) is sensitive to cosmic shear (2.6) through the ratio of the transverse and radial rescaling (e.g. steeper profiles enhance the asymmetry). In the limit of zero background shear, the ratio of rescaling factors tends to one, and the only difference w.r.t. FRW comes from the different relation between the angular diameter distance and the radial Hubble rate. Therefore, the information one obtains from the AP effect is *complementary* to the geometric mean distance given by Eq. (3.19), which only depends on the expansion, i.e. the product of the rescaling in the three spatial directions, and is unable to tell apart ξ_R from ξ_T . Therefore, the AP effect is not only able to distinguish FRW from LTB models, but could eventually allow to observationally discriminate between different LTB profiles.

4 Observational Data

The present analysis relies on the interplay between the cosmic distances obtained by type Ia supernovae and the distances *and* rescaling constraints from the baryon acoustic oscillation scale. SNe can be regarded as a standard candle and BAO as an standard ruler, which suffers additional effects due to the inhomogeneity. The measurement of the local expansion rate and the CMB peaks are also considered, their effect being to provide a calibration for the standard candles and rulers, respectively. However, the main result is independent of this calibration.

4.1 Type Ia Supernovae

The dimming of distant supernovae constitutes a solid probe of void models in the interval $0.01 \lesssim z \lesssim 1.5$, as the luminosity distance depends on all the parameters of the model in a nontrivial way. The difference in magnitude between each observed supernovae at redshift z_i and the theoretical expectation given by the luminosity distance $D_L(z)$ is

$$\mu^{\text{th}}(z_i) - \mu_i^{\text{obs}} = 5 \log_{10} \left(\frac{D_L(z_i)}{1 \text{Mpc}} \right) + 25 - \mu_0 - \mu_i^{\text{obs}} \equiv \Delta\mu_i - \mu_0, \quad (4.1)$$

where the last equality defines the value of $\Delta\mu_i$ which is used for the observational constraints. The quantity μ_0 depends on the intrinsic luminosity of the supernova explosions and will be allowed to take arbitrary values. Determinations of μ_0 will be used to constraint the local expansion rate (see below).

In addition to the intrinsic luminosity, two other unknown quantities are necessary to calibrate the supernovae measurements and obtain a standard candle. These are the stretch (the duration of the supernovae explosion) and the color (to account for dust extinction), which are assumed to be universal and introduce linear corrections on all the SNe

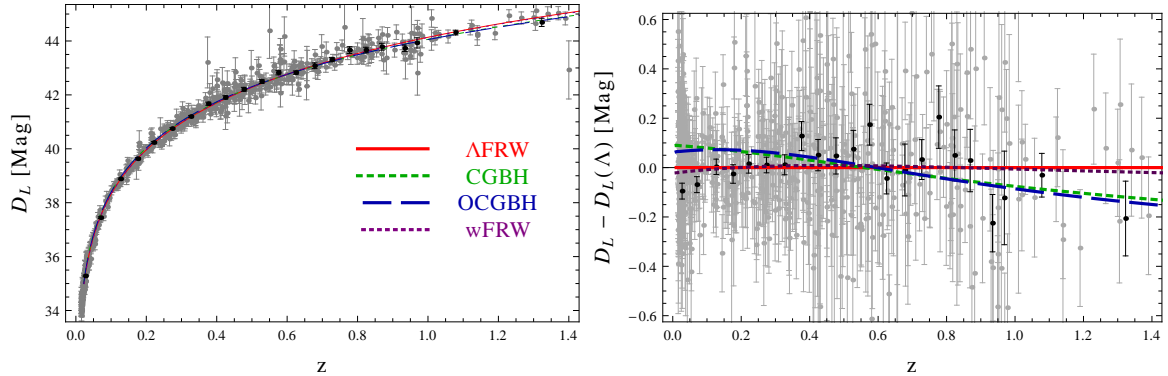


Figure 4. Supernovae data and luminosity distance. The gray points correspond to the Union 2 compilation [74] used in the computation of the likelihood. The black points correspond to a binning of the same data using the covariance matrix, and are intended only for visual aid. Color lines correspond to the minimum χ^2 models described in Section 5, rescaled with the optimal value of μ_0 , as described in the text.

$\mu_i^{\text{obs}} = \mu_{B,i} - \mu_0 + \alpha(s_i - 1) - \beta c_i$. These factors are calibrated by assuming an FRW- Λ CDM model, and should in principle be allowed to vary if the cosmology changes [13, 31]. However, the result of the analysis should not vary significantly since the LTB models we are considering usually give luminosity distance curves very similar to the standard model. The present analysis also includes the covariance matrix between the supernova data, which adds information about this calibration procedure by taking into account the covariance between supernovae with similar color and stretch.

The Union 2 supernovae compilation [74] consists in 557 SNe redshift-magnitude measurements after their lightcurves have been corrected for color and shape, shown in Figure 4. The likelihood is computed using the covariance matrix including systematic errors C_{ij}

$$-2 \log L_{\text{SNe}} = \chi_{\text{SNe}}^2 = \sum_{i,j} (\Delta\mu_i - \mu_0) C_{ij}^{-1} (\Delta\mu_j - \mu_0). \quad (4.2)$$

The above result depends on the actual value of the intrinsic luminosity μ_0 . Since it is unknown, the likelihood has to be maximized for each model with respect to μ_0 for each model under consideration [75]. Expanding the above expression and substituting back the value of μ_0 such that $\partial(\chi^2)/\partial\mu_0 = 0$, gives the optimal likelihood for each model

$$\chi_{\text{SNe}}^2 = \sum_{i,j} \Delta\mu_i C_{ij}^{-1} \Delta\mu_j - \frac{\left(\sum_{i,j} C_{ij}^{-1} \Delta\mu_j \right)^2}{\sum_{i,j} C_{ij}^{-1}}. \quad (4.3)$$

4.2 Local Expansion Rate

Recasting the expression for the luminosity distance (4.1) in units of H_0

$$\mu^{\text{th}}(z_i) = 5 \log_{10}(H_0 D_L(z_i)) + 25 - \mu_0 - 5 \log_{10}(H_0 [\text{Mpc}^{-1}]). \quad (4.4)$$

it is possible to see that the intrinsic luminosity μ_0 is degenerated with the Hubble constant for homogeneous models, for which cosmic distances only depend on it through a global H_0^{-1} factor. Although inhomogeneous cosmologies introduce additional scales and allow for

more involved dependences [26], the determination of the local expansion rate requires the knowledge of the intrinsic supernovae luminosity.

A recent measurement of the local expansion rate using Ia type supernovae yields a value $H_0 = 73.8 \pm 2.4 \text{ km s}^{-1} \text{ Mpc}^{-1}$ [58]. The supernovae intrinsic luminosity was measured using over 600 Cepheid stars from eight nearby galaxies in which type Ia supernovae have been observed. The Cepheids are calibrated comparing their luminosity to three different distance estimates: 1) the geometric distance to NGC 4258 as obtained from water masers orbiting its central black hole, 2) trigonometric parallaxes to Cepheid stars in the Milky Way and 3) relating the distance to the Large Magellanic Cloud obtained from eclipsing binaries. The local expansion rate is obtained by finding the best fit for a fiducial FRW model with $\Omega_M = 0.3$, $\Omega_\Lambda = 0.7$ to 253 low redshift type Ia supernovae ($z < 0.1$) using the measured intrinsic luminosities. In particular, the quoted value of H_0 is the average of the values obtained from the three different calibrations.

The dependence of the expansion rate with redshift in a LTB cosmology is in general very different than in the Λ CDM case, even for low redshifts $z < 0.1$. In order to reproduce the method used in [58] and provide a more fair comparison, we implement the constraints on the model using supernovae luminosities rather than the model parameter H_{in} . The value and the error in the luminosity were obtained by comparing the fiducial model fixing $H_0 = 73.8$ and 73.8 ± 2.4 to the Union2 data in the range $z < 0.1$ (195 SNe) and finding the value of μ_0^{obs} that gives the best fit, using equation (4.6) below. The result is

$$\mu_0^{\text{obs}} = -0.120 \pm 0.071. \quad (4.5)$$

The ‘‘predicted’’ intrinsic luminosity that can be compared to the observation is the best fit μ_0 found using the Union 2 data for the model under investigation

$$\mu_0^{\text{bf}} = \frac{\sum_{i,j} C_{ij}^{-1} \Delta \mu_j}{\sum_{i,j} C_{ij}^{-1}}, \quad (4.6)$$

using the distance modulus and the inverse covariance matrix of the data (see previous section and equations (4.1,4.2)). The associated likelihood is assumed to be Gaussian

$$\chi_{H_0}^2 = \frac{(\mu_0^{\text{bf}} - \mu_0^{\text{obs}})^2}{\Delta \mu_0^2}. \quad (4.7)$$

4.3 Baryon Acoustic Scale

Although the use of BAO to constrain LTB models has raised some criticism [26, 35], we will rely on our results from Section 3 showing that the baryonic features remain at constant coordinate positions to a good approximation and relating the transverse and radial BAO scales at different redshifts to the asymptotic values.

The WiggleZ collaboration [59] has measured the baryon acoustic scale at three different redshifts, complementing previous data at lower redshift obtained by SDSS and 6DFGS [76–78]. Their measurements are given in terms of the variable d_z , which in our model is computed as (3.17), or alternatively (3.19), (3.20).⁶ An additional point involving the purely angular correlation [60], from SDSS DR7 catalog in the range [0.5 – 0.6], has also been included at $z = 0.55$, to be compared to the theoretical θ_{BAO} prediction (3.13). All data points are summarized in Table 3 of [59] and displayed in Figure 5 together with the best fit models.

⁶The $A(z)$ variable lacks an interpretation in the context of an LTB inhomogeneous model. However, we checked that using this method with values $\Omega_m|_{A(z)} = \Omega_m(z=0)|_{\text{LTB}} \equiv \rho(r(0), t(0))/\rho(\infty, t(0))$ yielded consistent results.

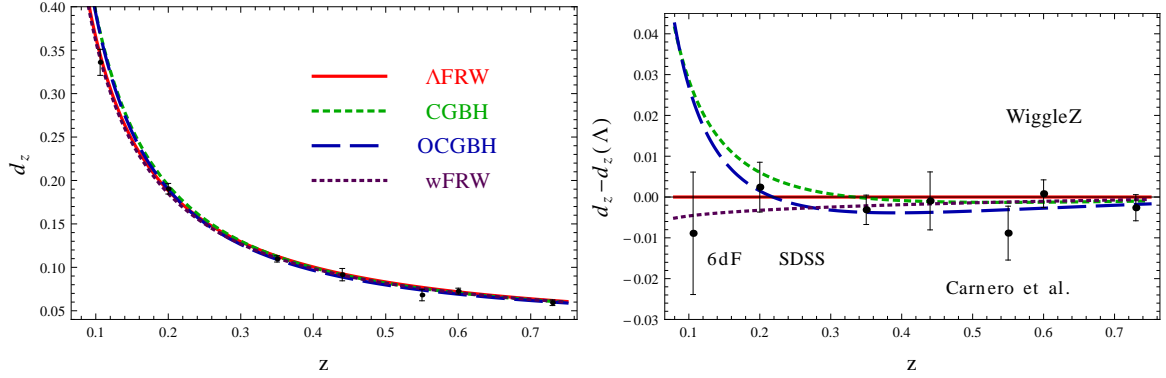


Figure 5. BAO data and d_z for the best fit models described in Section 5 and residuals with respect to Λ CDM. The point at $z = 0.55$ has been converted from angular to volume distance by means of a fiducial model.

	6dF	SDSS		WiggleZ			Carnero <i>et al.</i>	
z	0.106	0.2	0.35	0.44	0.6	0.73	z	0.55
d_z	0.336	0.1905	0.1097	0.0916	0.0726	0.0592	θ_{BAO}	3.90°
Δd_z	0.015	0.0061	0.0036	0.0071	0.0034	0.0032	$\Delta\theta_{BAO}$	0.38°

Table 1. BAO data. The first six data points are volume averaged and correspond to Table 3 of [59]. Their inverse covariance Matrix is given by (4.9). The last point corresponds to an angular measurement given in [60].

The choice of data is convenient because it covers the redshift range $z \leq 0.8$ with a regular spacing and the correlations are known (see below). The point at $z = 0.55$ was added to the ones summarized by the WiggleZ collaboration because it was obtained from the SDSS data in the interval $0.5 < z < 0.6$. Hence, it is independent of the measurements at $z = 0.2, 0.35$. Other available BAO scale determinations (e.g. references [73, 79–82]) would add points at intermediate redshifts with similar error bars and unknown covariances, and therefore we expect they will not increase the precision of the constraints. Determinations of the radial BAO scale [83, 84] are of particular interest to constrain inhomogeneous models [24, 28] due to the distinct radial rescaling factor (3.11). Nonetheless, they were not included in the analysis due to the lack of knowledge about the correlations with other datapoints.

The likelihood is given by

$$\chi_{\text{BAO}}^2 = \sum_{i,j} (d_i - d(z_i)) C_{ij}^{-1} (d_j - d(z_j)) + \frac{(\theta_{\text{BAO}}(0.55) - \theta_{\text{BAO}}^{0.55})^2}{\Delta\theta_{\text{BAO}}^2}, \quad (4.8)$$

where the indices i, j are in growing order in z , as in Table 1. For the first six points, C_{ij}^{-1}

was obtained from the covariance data in [59] in terms of d_z :

$$C_{ij}^{-1} = \begin{pmatrix} 4444 & 0. & 0. & 0. & 0. & 0. \\ 0. & 30318 & -17312 & 0. & 0. & 0. \\ 0. & -17312 & 87046 & 0. & 0. & 0. \\ 0. & 0. & 0. & 23857 & -22747 & 10586 \\ 0. & 0. & 0. & -22747 & 128729 & -59907 \\ 0. & 0. & 0. & 10586 & -59907 & 125536 \end{pmatrix}. \quad (4.9)$$

4.4 Cosmic Microwave Background

The cosmic microwave background radiation in LTB models has been actively investigated [50–54], as it constitutes the most solid piece of evidence for statistical isotropy and the most powerful tool in cosmological constraints. The obtention of precise constraints from the CMB is beyond the scope of this work and therefore only a relatively simple analysis based on the location of the first peaks will be employed, in order to give an idea of the effects of calibrating the standard rulers. This method yields weaker constraints than using the whole WMAP data and the spectra computed in linear perturbation theory, WMAP distance prior R, l_a, z_* [85] (See Section 5 and Figure 7) or other model independent determinations [86].

If our galaxy is located very close to the center of the void, the radiation coming from the CMB will be highly isotropic and therefore well described by the angular power spectrum C_l , with no direction dependence. As usual, it will display a characteristic pattern of peaks and troughs located at multipoles

$$l_m = (m - \phi_m) l_A, \quad (4.10)$$

where integer values of m labels the peaks, half integer values correspond to troughs, and ϕ_m are corrections that depends on the details of the cosmology *before* the recombination epoch. The overall factor is fixed by the *CMB acoustic scale*

$$l_A = \pi \frac{D_A(z_*)}{r_s(z_*)(1+z_*)^{-1}}, \quad (4.11)$$

determined by the ratio between the observed angular diameter distance until recombination and the sound horizon at that epoch. Further information on the cosmological parameters can be obtained by considering the relative heights of the acoustic peaks compared to the first one $H_a = C_{l_a}/C_{l_1}$.

The decoupling epoch occurs at an early time when the universe is very homogeneous and the primary anisotropies are produced on our past lightcone at a radius much larger than the size of the void $r(z \sim 1100) \gg R$. In this case the pre-recombination physics is effectively the same as in a homogeneous universe, and we can assume that the relative peak positions $(m - \delta\phi_m)$ and heights H_a are those of a FRW universe with the effective asymptotic values of the LTB model discussed in section Section 3.2.⁷ On top of modifying these asymptotic parameters, the only effects from the void will be to shift the peaks by varying the acoustic scale l_A through the angular diameter distance $D_A(z_*)$. Our analysis neglects secondary contributions such as the integrated Sachs Wolf effect on the lower multipoles or the action of gravitational lensing, which affects the relative heights of the peaks. Furthermore, we will assume no radiation contribution to the angular distance to recombination.⁸

⁷Variations in the effective CMB temperature have not been considered because for the profiles under consideration (compensated voids) there is no significant departure from $T_0 = 2.725K$ [12, 32].

⁸See references [52, 87, 88] for discussions on radiation in the context of LTB models.

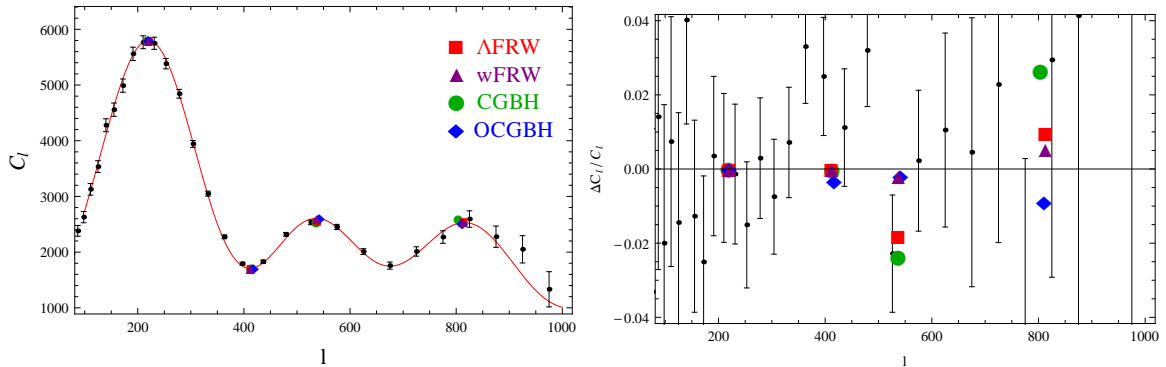


Figure 6. CMB spectrum. Black dots and error bars correspond to the binned WMAP7 data and the red line is the CMB only best fit for Λ CDM [89]. The color points are the reconstructed positions of the peaks using the method described in Section 4.4 for the minimum χ^2 models (Section 5). For visualization aid, the WMAP best fit height has been assumed for the first peak, which is equivalent to a normalization, and the first through due to the lack of a fitting formula (The residuals in $H_{3/2}$ are due to the propagation of $l_{3/2}$). Although the formulae do not exactly recover the values computed in linear perturbation theory, they fall within the assumed errors (1% for l_1 , 3% for the rest). Note that the LTB models require values ($f_b \approx 0.7$, $n_s \approx 0.6$ that depart considerably from the standard model (Section 5). More precise constraints taken into account the full spectrum would considerably lower the quality of the fit.

In order to compare the theoretical predictions and the observations we will follow the approach described by Marra and Pääkkönen [32]. The corrections to the peak locations ϕ_m and heights depend on the effective parameters through the ratio of matter-radiation density and recombination and the physical baryon density $\Omega_m h^2$, as well as the spectral index n_s that characterizes the power spectrum of primordial perturbations. Note that relaxing the common assumption of a nearly scale invariant primordial spectrum considerably reduces the tension between CMB and the local expansion rate [31]. Accurate fitting formulae in terms of these quantities are provided in reference [90] for the recombination epoch z_* and the sound horizon $r_s(z_*)$, reference [91] for l_m with $m = 1, \frac{3}{2}, 2, 3$ and reference [92] for the relative height H_a of the second and first peak $a = 2, 3$. Figure 6 shows the location of the peaks reconstructed using this method.

The total likelihood is given by

$$\chi_{\text{CMB}}^2 = \sum_{m \in \{1, \frac{3}{2}, 2, 3\}} \frac{(l_m^{\text{obs}} - l_m^{\text{LTB}})^2}{2\sigma_{l_m}^2} + \sum_{a \in \{2, 3\}} \frac{(H_a^{\text{obs}} - H_a^{\text{LTB}})^2}{2\sigma_{H_a}^2}, \quad (4.12)$$

where the positions and heights of the peaks are those matching the WMAP 7 year best fit model. As in reference [32], we have taken the errors to be of 1% for the position of the first peak and 3% for the remaining parameters. It is important to note that this likelihood analysis is very simplified and its main aim is to provide an insight on how the information from the CMB helps to sharpen the BAO constraints by fixing the initial size of the standard ruler.

5 Analysis and Results

In order to constrain the parameter space and address the viability of the different models, we run several Markov Chain Monte Carlo (MCMC) analysis using a modified version of the publicly available code CMBEasy [93], which includes the integration of the coordinates over the lightcone and the computation of the cosmological observables in the LTB model described in sections 3 and 4. CMBEasy’s built in MCMC driver establishes the convergence of the chains through the test of Gelman and Rubin [94], which establishes the length of the burn-in sequence and freezes the step-size, which is a necessary condition for the convergence of the MCMC algorithm [95]. In addition, the chains were monitored manually to ensure a proper sampling of the parameter space.

Additionally to the CGBH and the OCGBH models described in section 2.1, a Λ CDM model and a wCDM model with constant equation of state were studied using the same data. Separate runs were performed for each of the displayed contours corresponding to the constraints of the separate sets (CMB, BAO, SNe) as well as the combined constraints H0+BAO+CMB+SNe. For the inhomogeneous models the additional combinations H0+SNe and BAO+CMB were considered, which combine the information of standard candles/rulers together with their calibrations (as opposed to the SNe/BAO-only). All the runs used flat priors on the model parameters, which are given in Table 2.

FRW MODELS

H_0 [Mpc/km/s]	Ω_M	Ω_Λ	$-w$	$100f_b$	n_s
30 – 90	0.05 – 0.8	0 – 1.2	0 – 5	1 – 25	0.05 – 1.3

GBH-LTB MODELS

H_{in} [Mpc/km/s]	Ω_{in}	Ω_{out}	R [Gpc]	ΔR [Gpc]	$100f_b$	n_s
30 – 90	0.01 – 0.5	0.1 – 1	0 – 5	0.5 – 5	1 – 25	0.05 – 1.3

Table 2. Priors on the model parameters used in the MCMCs. In order to facilitate the comparison between the two LTB models, for the CGBH profile we have fixed the value of $H(r = 0) \equiv H_{\text{in}}$ at the center of the void instead of the more obscure parameter H_0 . Ω_{out} and w are only varied in the OCGBH and wCDM models.

The results from the combined constraints can be seen in Table 3. Figures 7, 8, 9 and 10 show the two-dimensional marginalized likelihood contours obtained from the individual and combined data sets. Our discussion starts by considering the homogeneous reference models. Then the results for the inhomogeneous CGBH and OCGBH profiles will be addressed, and the goodness of fit of the different models compared using different criteria.

5.1 Homogeneous models

For Λ CDM the recovered parameters are in good agreement with previous results. However, the region compatible with CMB data (first plot in Figure 7) is broader than usual around the flatness line. This lack of precision is caused by the partial use of the CMB data (i.e. only the peaks instead of the whole C_l spectrum), together with the broad parameter priors allowed. When combined with other measurements, it also affects the recovered value of the

ΛCDM MODEL

	H_0 [Mpc/km/s]	Ω_M	Ω_Λ	$100f_b$	n_s
All - Min χ^2	70.7	0.28	0.72	17	0.97
Marginalized	$70.3^{+1.7}_{-1.5}$	0.27 ± 0.03	0.73 ± 0.05	17 ± 0.04	$0.99^{+0.06}_{-0.09}$

wCDM MODEL

H_0 [Mpc/km/s]	Ω_M	Ω_Λ	w	$100f_b$	n_s
72.8	0.32	0.66	-1.26	12	0.87
73.5 ± 2.3	0.33 ± 0.04	0.64 ± 0.06	$-1.26^{+0.17}_{-0.22}$	$0.10^{+0.03}_{-0.02}$	$0.82^{+0.08}_{-0.06}$

ASYMPTOTICALLY FLAT CONSTRAINED GBH MODEL (CGBH)

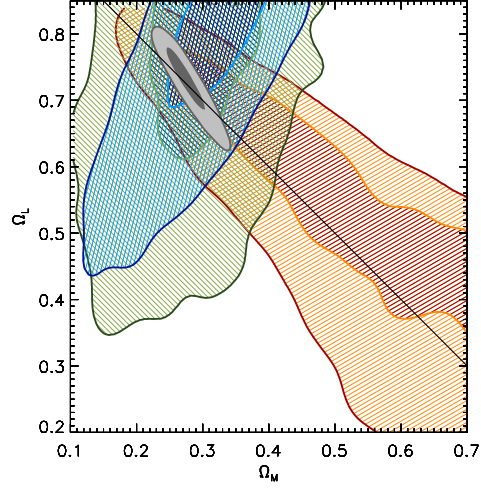
	H_{in}	Ω_{in}	R [Gpc]	dR [Gpc]	$100f_b$	n_s
All - Min χ^2	66.4	0.21	0.02	2.78	7.7	0.74
Marginalized	66.0 ± 1.4	0.22 ± 0.04	$0.18^{+0.64}_{-0.18}$	$2.56^{+0.28}_{-0.24}$	7.7 ± 0.4	0.74 ± 0.03
BAO+CMB	61.6 ± 2.4	$0.32^{+0.06}_{-0.04}$	$3.92^{+0.48}_{-3.71}$	$2.76^{+0.50}_{-0.88}$	7.8 ± 0.8	0.73 ± 0.04
SNe+H0	74.0 ± 2.6	0.07 ± 0.04	$1.95^{+1.22}_{-1.82}$	$3.19^{+1.63}_{-1.66}$	-	-

ASYMPTOTICALLY OPEN CONSTRAINED GBH MODEL (OCGBH)

H_{in}	Ω_{in}	Ω_{out}	R [Gpc]	dR [Gpc]	$100f_b$	n_s
71.8	0.21	0.87	0.30	1.48	6.3	0.67
71.1 ± 2.8	0.22 ± 0.04	0.86 ± 0.03	$0.20^{+0.87}_{-0.19}$	$1.33^{+0.36}_{-0.32}$	6.2 ± 0.5	0.68 ± 0.03
$63.8^{+4.2}_{-2.8}$	0.35 ± 0.06	$0.98^{+0.02}_{-0.11}$	$0.72^{+2.5}_{-0.67}$	1.79 ± 0.89	6.8 ± 0.9	$0.69^{+0.05}_{-0.03}$
$73.4^{+3.1}_{-2.1}$	0.06 ± 0.04	$0.89^{+0.09}_{-0.25}$	$0.80^{+1.66}_{-0.74}$	$1.63^{+2.04}_{-0.79}$	-	-

Table 3. Parameters from the MCMC including H0+SNe+BAO+CMB discussed Section 5. The first lines correspond to the minimum χ^2 models, while the second lines corresponds to the best fit model with one sigma errors after marginalizing over the remaining parameters. Note that since the LTB models do not give good fits to the data the errors are apparently very small (see Figures 7, 8, 9 and 10). For the sake of comparison, in the case of the LTB models the results from the separate fits using BAO+CMB and SNe+H0 have been added (third and fourth lines).

Λ CDM MODEL



wCDM MODEL

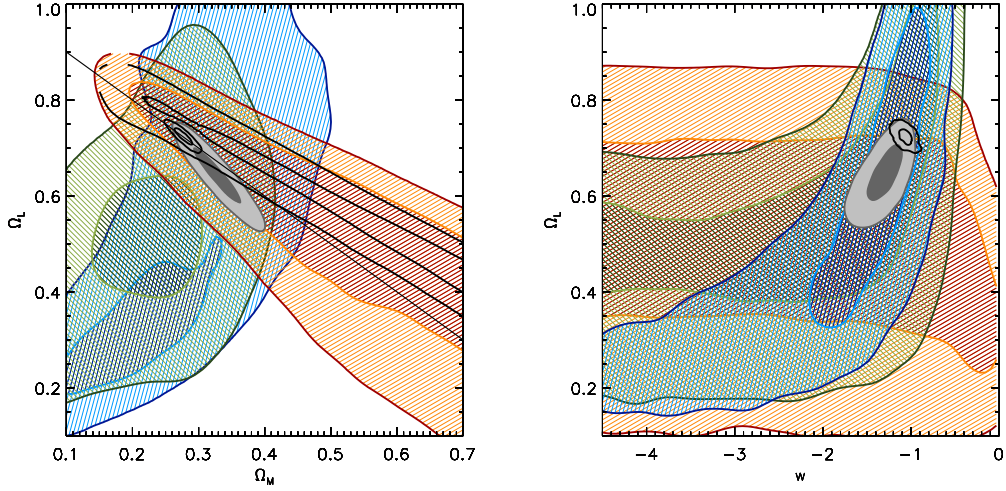


Figure 7. One and two sigma regions for the marginalized likelihood function corresponding to the Λ CDM and wCDM homogeneous model as obtained from BAO (green), CMB (Orange) and SNe (blue). Gray contours are the combined constraints H0+BAO+CMB+SNe. Note that the CMB compatible regions are much broader than usual due to the simplification of the method. Black unfilled lines in the wCDM plots correspond to using the WMAP distance prior R, z_*, l_A [85] combined with H0+BAO+SNe or individually (shown only in the $\Omega_\Lambda - \Omega_m$ plane), which recover the standard results.

curvature $\Omega_k = 0.003_{-0.025}^{+0.015}$, which is still very close to flat but has larger error bars than usual. In a computation taking into account the full WMAP7 data, a deviation with respect to the measured values of the peak positions would also displace many of the intermediate points and cause a more dramatic decrease of the likelihood, leading to tighter bounds.

The weakness of the CMB constraints is reflected again in the recovered values for the Λ CDM model (second and third plots in Figure 7). In this case all the parameters except H_0 , which is independently constrained by the nearby expansion rate, depart considerably from the standard ones. These allow for lower values of the baryon fraction and the spectral index, which in turn increase the matter fraction and decrease the dark energy content. A very dramatic consequence of the weakness of these constraints can be seen in the recovered value of the curvature $\Omega_k = 0.04 \pm 0.02$, two sigma away from flatness. The low value of $\Omega_\Lambda \approx 0.62$ is then compensated with an anomalously low equation of state $w \approx -1.34$.⁹

Note also how the BAO and SNe contours span a similar region in both cases. This is a consequence of them being determined by measurements of standard rulers and candles with *arbitrary* calibration, over a comparable redshift interval (due to the new BAO data provided by the WiggleZ collaboration, up to $z \sim 0.8$). Since in FRW both datasets depend only on the same distance-redshift relation and are consistent with each other, they yield basically the same information and the recovered regions overlap.

5.2 Inhomogeneous models

Discrepancies between the different datasets are encountered for both models regarding the matter content and the expansion rate at the center of the void, as can be seen in Figures 8, 9, 10. This becomes particularly clear for the $\Omega_{\text{in}} - h_{\text{in}}$ plane.

The most severe problem for both models is the existing tension regarding the value of Ω_{in} determined from BAO and SNe, which differs by roughly 3σ for the two models (see figures 8, 9). For example, the asymptotically flat model (CGBH) the BAO-only 1D marginalized likelihood yields $\Omega_{\text{in}} = 0.28_{-0.05}^{+0.06}$ (1 sigma), a much higher value than determined by SNe $\Omega_{\text{in}} = 0.07 \pm 0.04$. This discrepancy is showing how the distance redshift relation necessary to explain the supernovae dimming is incompatible with the stretch of the standard ruler inside the void due to the inhomogeneous rescaling discussed in Section 3. The low value of Ω_{in} necessary to fit SNe observations increases the expansion rate and therefore stretches the BAO scale considerably near the center, making it incompatible with the observed values at higher redshift. This is a purely geometric discrepancy, valid for arbitrary calibration of the standard candles and rulers, and is completely independent of the dynamics originating the characteristic length. Figures 4, 5 show how the best fit models represent a compromise that fails to fit both datasets at low redshift, where the BAO rescaling (Fig. 3) is largest.

Naturally, the tension becomes more dramatic when the SNe data are compared to the BAO+CMB combination, because the CMB effectively reduces the allowed range of the initial BAO scale by constraining H_{in} , f_b and Ω_{out} . The independence of the constraints on the initial BAO scale is the reason why the asymptotically open model (OCGBH) does not ease the tension between BAO and SNe. This is partly because the apparent freedom gained

⁹The discrepancies disappear when the WMAP7 distance prior R, z_*, l_A [85] are used instead of the peak positions (black, unfilled contours in Figure 7), recovering $\Omega_k \approx 0$ and $w \approx -1$. These quantities have been very accurately determined by the WMAP collaboration using the full CMB spectrum, and are able to break the degeneracies in the model (e.g. the baryon fraction). Although they are considerably more precise than the CMB peak information we used (described in Section 4.4), the WMAP distance prior can not be directly applied to inhomogeneous models (e.g. LTB models with decoupling redshifts $z_* \gtrsim 1110$ considerably higher than the standard value $z_* = 1091.3 \pm 0.9$ can yield a good fit [50]).

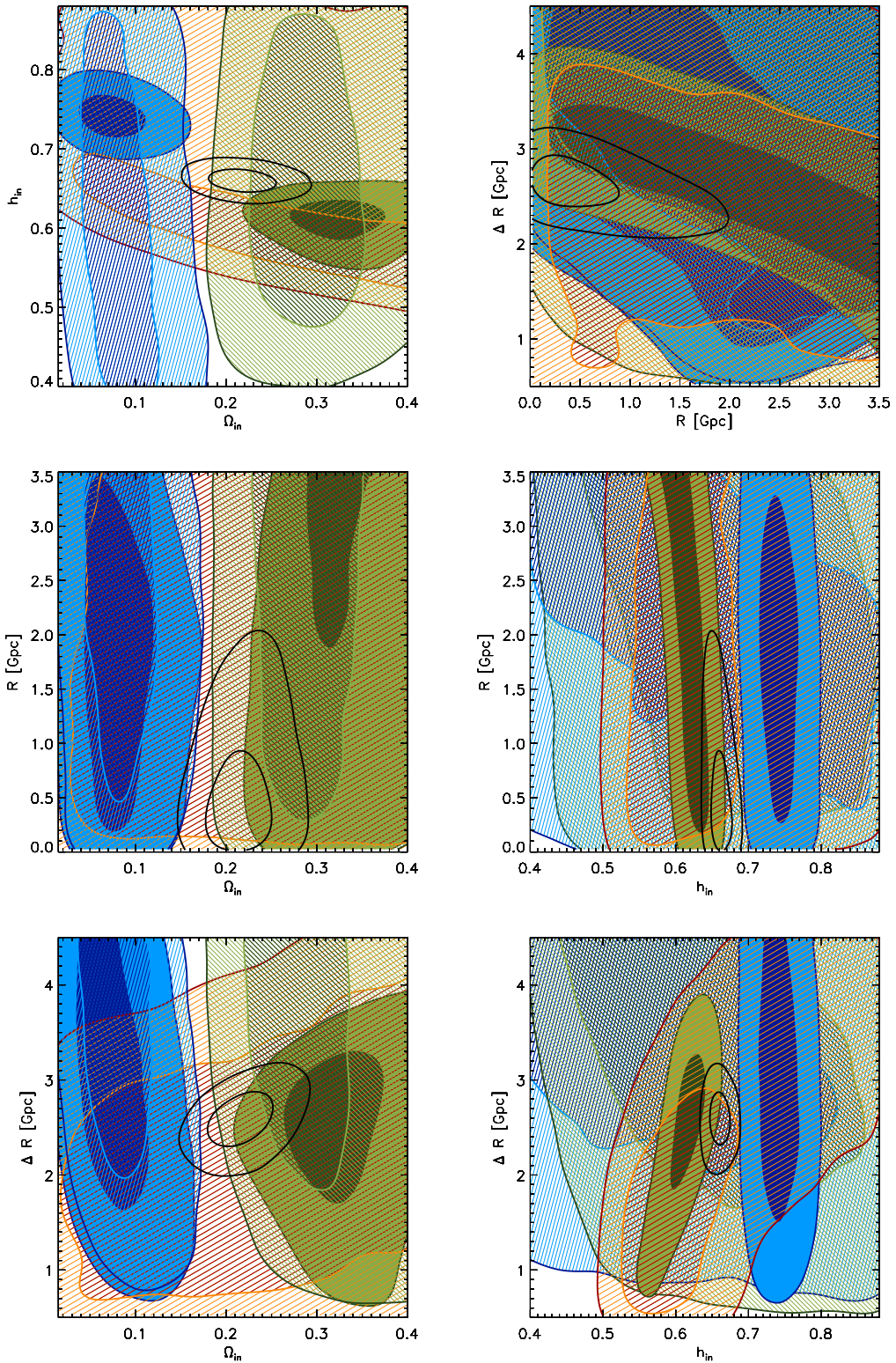


Figure 8. CGBH model. One and two sigma regions for the marginalized likelihood function as obtained from BAO (green), CMB (Orange) and SNe (blue). The filled contours represent the combined constraints using SNe+H0 (blue) and BAO+CMB (green). The black lines correspond to the combined data BAO+CMB+SNe+H0.

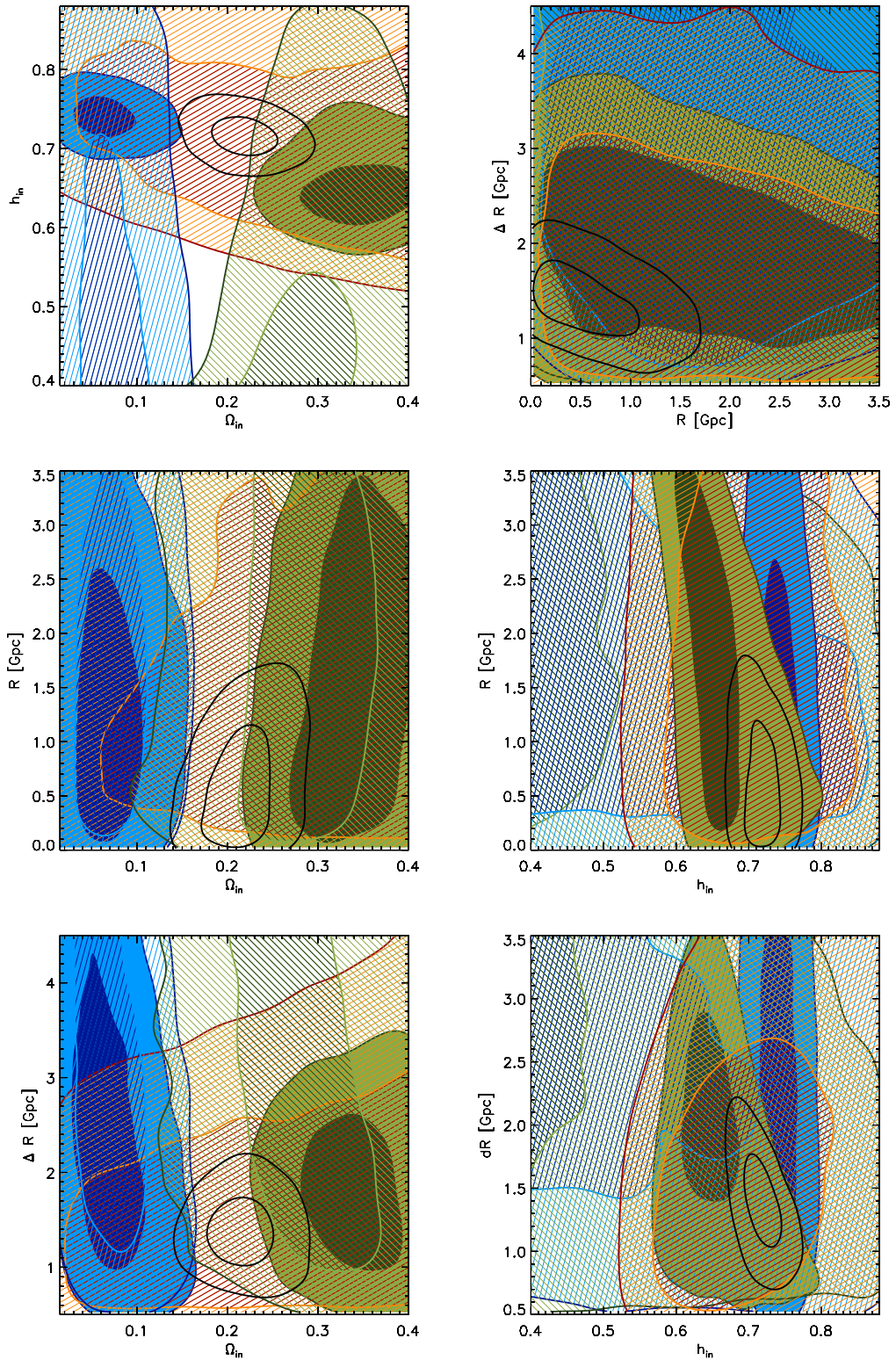


Figure 9. OGBH model. One and two sigma regions for the marginalized likelihood function as obtained from BAO (green), CMB (Orange) and SNe (blue). The filled contours represent the combined constraints using SNe+H0 (blue) and BAO+CMB (green). The black lines correspond to the combined data BAO+CMB+SNe+H0.

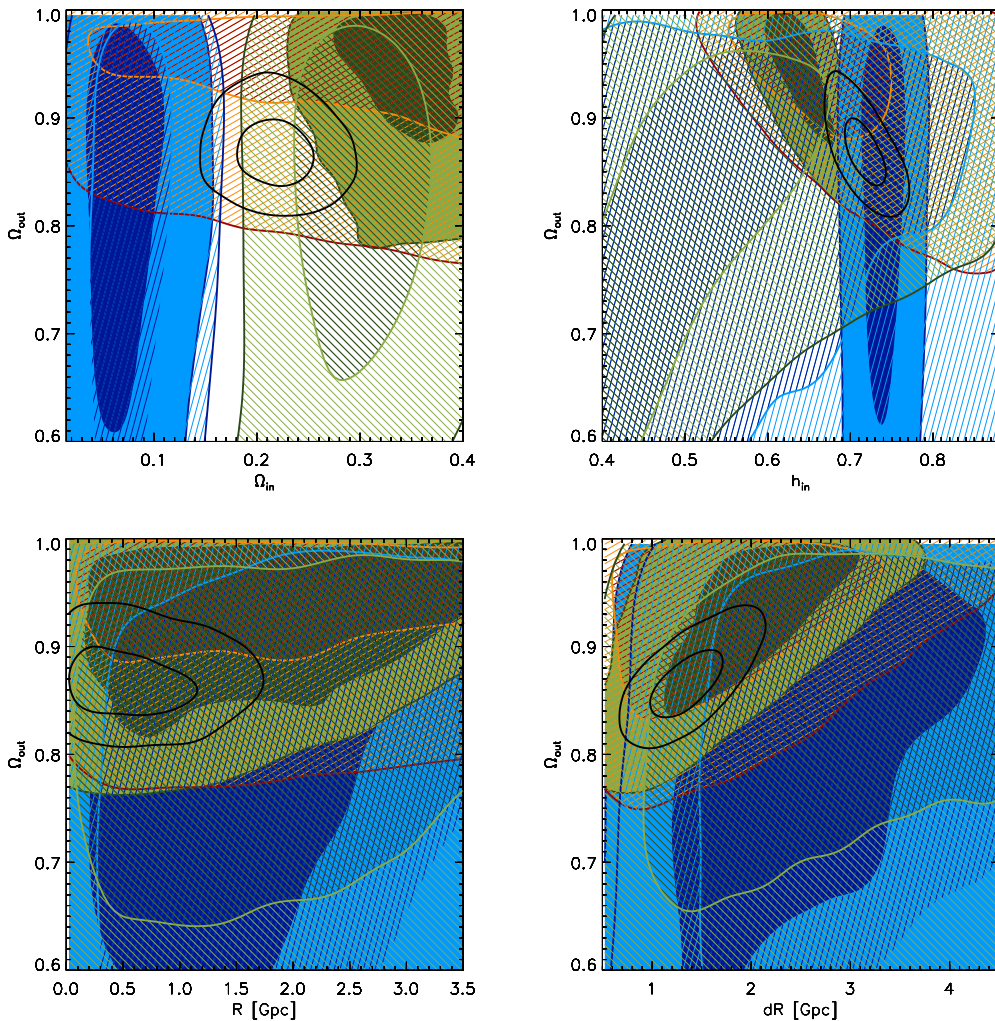


Figure 10. Continuation of Figure 9.

from allowing Ω_{out} to vary does not provide essentially different values of the asymptotic BAO scale, already ensured by the freedom in f_b . The other reason is that neither SNe nor BAO-only constraints seem to depend on the value of Ω_{out} . We can regard the dashed green and blue contours in Figures 8, 9, 10) as the purely geometric constraints for *arbitrary* values of the standard rulers/candles, while the filled green and blue contours would correspond to adding priors to those calibrations.

The asymptotically flat model (CGBH) also shows a tension between the value of H_{in} determined by H0+SNe and CMB+BAO, both being discrepant at 3σ . Note that the tension is manifest even using very simplified CMB data, although these yield much looser constraints than the full C_l spectrum. In the asymptotically open model, the additional freedom achieved allows to recover agreement by reducing the value of Ω_{out} , yielding a concordant value for H_{in} from the different datasets. However, the tension would reappear in more a thorough analysis including the full CMB power spectrum data, which typically require $h_{\text{in}} \sim 0.4 - 0.5$

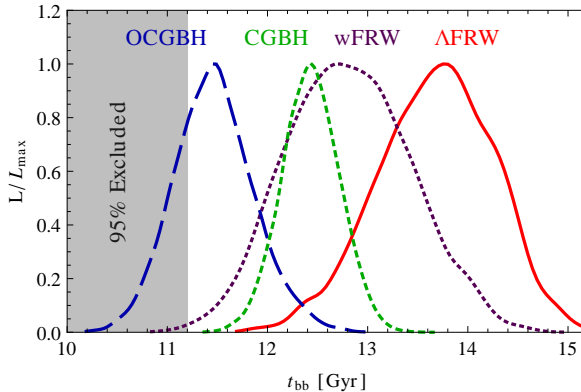


Figure 11. Age of the universe for the best fit models. The curves correspond to marginalization of the MCMC chains over the (homogeneous) Big Bang time (note that it is a derived quantity rather than a parameter varied in the exploration). The gray area shows the region excluded by the age of Globular Clusters in the Milky Way.

[28]. This increase in the local expansion rate also reduces the age of the universe, which is proportional to $H_0(r)^{-1}$. Although it has not been explicitly accounted for in the MCMC, Figure 11 shows how models with a higher expansion rate enter in tension with the limits on the age of the universe obtained from Globular Clusters [96], posing yet another difficulty for this type of models.

The recovered values of the baryon fraction and the spectral index, mainly determined by the CMB, are much lower than in standard cosmologies. This trend agrees with previous studies in which compensated voids are constrained using the full CMB [12]. We note that these features are not relevant to our discussion because 1) the main results are geometric and do not depend on the details of the CMB physics and 2) the obtained values of f_b, n_s rely on a simplified treatment of the CMB peaks.

The best fit models turn out to be rather cuspy, as can be seen in the preference towards $R \approx 0$ Gpc in both the asymptotically flat and open voids. Since the fit is not very good and the individual observations are not very restrictive by themselves (including the combinations BAO+CMB, SNe+H0), this feature might well be due to a compromise between the different datasets, and could be related to the fact that cuspy voids achieve better resemblance to an accelerating universe at low redshift [7]. In this case, the size of the void is given by the steepness of the inhomogeneity ΔR , which acquires a value ~ 2.5 Gpc in the flat case but a smaller value ~ 1.5 Gpc in the asymptotically open case. Again, the individual data sets do not yield significant enough information about the value of $R, \Delta R$. Other than the smallness of the asymptotically open void and the better agreement it gives on the value of H_0 , there is no significant difference between the two models.

5.3 Model comparison

We now proceed to compare the different models under several criteria. The tensions between the different datasets (Figures 8, 9 and 10) and the poor fit to SNe and BAO (Figures 4 and 1) will be reflected in poorer figures with respect to the homogeneous models. Furthermore, inhomogeneous models will be additionally penalized because they have a larger number of

	CGBH	OCGBH	Λ CDM	wCDM
Union SNe	539.94	539.06	530.70	530.40
Hubble μ_0	6.97	0.38	2.17	0.14
6dF	5.35	4.73	0.35	0.09
SDSS	0.73	0.04	1.29	1.24
WiggleZ	0.65	1.20	0.93	0.63
Carnero et al.	0.78	0.12	0.61	0.34
Total BAO	7.51	6.09	3.18	2.30
Peak positions	0.87	0.30	0.96	0.07
Peak heights	1.13	0.11	0.24	0.04
Total CMB	2.00	0.41	1.20	0.11
Total χ^2	+19.89	+9.40	536.56	-3.62
# free parameters	6	7	5	6
χ^2 /d.o.f.	0.985	0.968	0.948	0.943
Akaike IC (5.1)	+22	+13	546.6	-1.6
Bayesian IC (5.2)	+26.2	+15.7	568.3	+2.7
Bayes factor (5.4)	+10	+6	282.2	+2.6

Table 4. χ^2 contributions to the maximum likelihood models as found by the MCMCs with H0+BAO+CMB+SNe and results from different model comparison criteria discussed in Section 5.3. The values χ^2 as well as the model comparison criteria are given show the total value for the Λ CDM best fit, while the other models are given relative to those (minus values are favoured w.r.t. the concordance model, while positive values are disfavoured). The Bayes factor is given by the difference in $-\log E$ (5.4).

parameters. Table 4 shows the χ^2 values associated to the different observations and the total values, as well as the result of the different judgment gauges discussed below.

The standard frequentist analysis of parameter estimation, given a set of data, is not very useful for model selection, since it is difficult to compare models with different number of parameters. For instance, the usual method of comparing minimum χ^2 per effective degree of freedom normally misses the point and is not very decisive, as can be seen in the very close values achieved by the different models. Other methods to decide which model gives the best description include various Information Criteria which additionally penalize models described by more parameters. Such include the (corrected) Akaike Information Criterion (*AIC*) [97] and Bayesian Information Criterion (*BIC*) [98], given by

$$AIC = \chi_{\min}^2 + 2k + \frac{2k(k-1)}{N-k-1}, \quad (5.1)$$

$$BIC = \chi_{\min}^2 + k \ln N, \quad (5.2)$$

where k is the number of free parameters of a given models and N the number datapoints used in the constraints. The Bayesian evidence

$$E(\mathbf{D}|\mathcal{M}) = \int du \mathcal{L}(\mathbf{D}|u, \mathcal{M}) \pi(u, \mathcal{M}), \quad (5.3)$$

is given by the integral of the likelihood $\mathcal{L}(\mathbf{D}|u, \mathcal{M})$ over the values of the model parameters u allowed by the priors $\pi(u, \mathcal{M})$. The computation of the Bayesian evidence is difficult in

general, therefore, we will use a simple expression which can be obtained provided that the likelihood is a single isolated peak, far from the edges of the prior ranges [23]

$$-\ln E = -\ln \mathcal{L}_{\max} + \ln A + \sum_i^n \ln(u_i^{\max} - u_i^{\min}), \quad (5.4)$$

where A is the normalization of the likelihood, and $[u_i^{\min}, u_i^{\max}]$ is the range of parameter u_i allowed in the MCMC exploration (assuming a flat priors), $i = 1 \dots n$. Moreover, for the case of a Gaussian likelihood,

$$\mathcal{L}(u) = A \exp \left[-\frac{1}{2} \mathbf{u}^T C^{-1} \mathbf{u} \right], \quad (5.5)$$

we find $A = (2\pi)^{-n/2} / \sqrt{\det C}$, where C is the covariance matrix and $x_i = u_i - \bar{u}_i$. It is clear that whenever the prior ranges are too big for the likelihood, the Bayesian evidence is penalized. An estimate of the covariance matrix can be obtained assuming that the obtained parameters are independent from each other. In that situation, the covariance matrix is given by the square of the one sigma allowed ranges in each parameter and the determinant becomes $\det C = \prod_i \sigma_i^2$, where we take the average between the upper and lower bounds given in Table 5. The determinant computed using the eigenvalues of the covariance matrix used in the MCMC sampling yields similar results.

The bottom part of Table 4 shows similar values for the homogeneous models, but the preferred one depends ultimately on the chosen criterion. It is interesting to note that the Bayes factor favors the simpler Λ CDM with a difference of 2.6, despite the slightly better χ^2 fit of the wCDM model. This difference is due to the presence of an additional parameter, w , together with the large prior postulated for it, $[-5, 0]$, relative to the 1σ region, $\Delta w \approx 0.2$.

The logarithm of the Bayes factor for the LTB models w.r.t. to the fiducial Λ CDM is 10 and 6, for the asymptotically flat and open GBH inhomogeneous models respectively, due to the bad fit and the larger parameter range explored. Although the asymptotically open model yields a better Bayes factor, even with an additional parameter, both are strongly disfavored according to Jeffreys' scale, since the difference in the logarithm of the Bayes factor is higher than 5. The Akaike and Bayesian Information Criteria also prefer the homogeneous model, the rejection being significantly stronger for the asymptotically flat case due to the extra tension in the local expansion rate. Increasingly accurate data have significantly worsened the fits of inhomogeneous universes, which were compatible just few years ago (c.g. reference [23]).

6 Discussion

In this paper we presented new constraints on inhomogeneous Lemaître-Tolman-Bondi models in the light of the most recent cosmological data, focusing profiles of the GBH type with a space-independent Big Bang and baryon fraction. The inclusion of higher redshift BAO data together with type Ia supernovae allows to reject the models based only on BAO and SNe, independently of other observational data such as the CMB. Additionally, a model independent method to constraint the local expansion rate through a prior on the supernovae luminosity was introduced.

The physical BAO scale at early times was computed in terms of the asymptotic value and then projected to different redshifts using the background LTB metric. This method is

justified due to the existence and stability of constant coordinate geodesic solutions, which are expected to be followed by baryonic overdensities in position space. In addition to the time evolution, the BAO scale is shown to become inhomogeneous and anisotropic due to the different expansion rates in the radial and transverse directions. The dependence of the observed BAO scale on both the cosmic distances *and* the evolution of the scale factor leads generically to different predictions than pure distance indicators such as SNe. The departure is largest near the center of the void, precisely because there is less matter to slow down the expansion that drives the growth of the BAO scale. Ultimately, the difference between the two distances can be regarded as a concrete realization of more general tests of the Copernican Principle [99].

The addition of BAO data at higher redshifts increases considerably their constraining power in this type of models because they help to fix the asymptotic value. The result represents a new drawback for this type of models, as the value of the local matter density $\Omega_{\text{in}} \gtrsim 0.2$ preferred by BAO is about 3σ apart from the value $\Omega_{\text{in}} \lesssim 0.18$ found using Supernovae, as can be inferred from Figures 8 and 9. The tension between the two datasets persists when asymptotically open models are studied, and worsens when the information from the CMB is added, since it constraints the parameters involved in the acoustic scale determination ($f_b, h, \Omega_{\text{out}}$). Asymptotically flat LTB models show an additional tension regarding the value of the local Hubble rate when CMB and BAO are combined. Allowing $\Omega_{\text{out}} \leq 1$ relaxes this incompatibility, but we expect it to re-emerge in a more detailed analysis of the CMB. Additionally, larger values of the expansion rate might render the universe too young to account for the ages of stars in globular clusters. The adiabatic GBH models fail to simultaneously fit the data, and a Bayesian analysis shows that they are ruled out at high confidence.

The above results were obtained for a particular choice of the matter profile. However, the difficulties of the model are manifest in the determined value of matter contrast at the center of the void, while the remaining parameters are poorly constrained by individual datasets. The departure between cosmic rulers and candles becomes most severe at the center of the void, and we expect that $\Omega_{\text{in}} = \lim_{r \rightarrow 0} \Omega_M(r)$ captures this tension regardless of other features. Since Ω_{in} can be defined for any LTB model regardless of the parameterization, it is reasonable to expect this result to hold for *all* large void models with space-independent Big Bang and baryon fraction. Nonetheless, we have to keep in mind that the SNe and BAO constraints depend on all the parameters through the distance determinations and the evolution of the BAO scale up to a certain redshift, and therefore different shapes for the profile might soften the tension between the two datasets.¹⁰

Similarly to the dependence of CMB constraints with the primordial power spectrum [31], it is conceivable that fine tuned initial perturbations could be used to reconcile the BAO observations with SNe in adiabatic voids. However, such conditions would not only need to *provide* an enhanced scale to explain the observed feature in galaxy correlation, but also to *hide* the actual BAO scale that would naturally form due to the existence of a preferred scale (the sound horizon at the recombination epoch). On top of this challenging task, the *fake* BAO scale should be shorter near the center to compensate the inhomogeneous growth and fit the observations, therefore requiring some amount of radial dependence that would be at odds with the (quasi) homogeneous initial state.

¹⁰Recently, genetic algorithms were used to analyze the sensitivity of LTB model profiles to the data regardless of the parameterization [100]. The results were not conclusive with respect to the shape of the void profile.

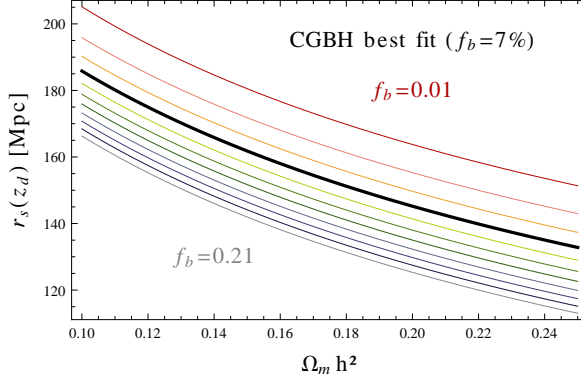


Figure 12. FRW, coordinate baryon acoustic scale $r_s(z_d)$ as a function of the physical matter density $\Omega_m h^2$ for different values of the baryon fraction. The mass of the baryons acts lowering the speed of sound in the baryon-photon fluid, and therefore increasing their amount reduces the resulting acoustic scale, which is related to the sound horizon. An LTB model with a higher baryon fraction near the center might render the BAO and SNe observations compatible by lowering the value of $d_z \propto r_s(z_d)$ near the center of the void (see Figure 5).

The effects of the inhomogeneity on the BAO scale are unavoidable. Even if a different void profile might yield a slightly better fit, more precise data e.g. from future surveys such as EUCLID [101] will eventually be able to distinguish adiabatic LTB models from the homogeneous case regardless of the shape of the inhomogeneity. Together with the remaining observational problems for large void models with space-independent Big Bang, this sets the stage for abandoning the adiabatic assumption. A scenario with inhomogeneous bang time would require more careful considerations on the origin of the BAO scale to account for the early time inhomogeneity, but it is still possible that the freedom gained from decoupling $H_0(r)$ from $\Omega_M(r)$ renders BAO and SNe observations compatible, although the modulation of the Hubble rate is restricted by the local and asymptotic values, fixed by SNe luminosity priors and the CMB.¹¹

A simpler possibility to reconcile SNe and BAO would be to allow for large scale baryon isocurvature modes, and induce a radial dependence on the early time BAO scale through a non-constant baryon to matter ratio $f_b(r)$.¹² Figure 5 suggests that lowering the *local* value near the center of the void would give a nicer fit to the observations, since the value of $d_z \propto r_s/D_V$ is proportional to the physical acoustic scale. A higher baryon fraction acts reducing the speed of sound of the baryon-photon fluid, therefore shortening the sound horizon that determines the observed BAO scale (see Figure 12). Adding more baryons at the center of the void would provide the necessary freedom to compensate for the inhomogeneous expansion and render the model phenomenologically viable, although more involved and less appealing.¹³

To summarize, we have shown how the BAO scale, acting as a standard (but evolving)

¹¹Models with arbitrary $H_0(r)$ also predict a too large kinematic Sunyaev-Zel'dovich effect [36, 54]. It might be still possible to avoid these constraints by including an additional baryon to photon profile $\eta(r)$ [56].

¹²A related alternative has been explored as way to explain the observed abundances of primordial nuclei and attempt to solve the primordial lithium problem [17].

¹³Baryon isocurvature modes are severely constrained by CMB observations [85, 102]. However, these constraints apply to scales much smaller than the size of the void.

ruler and the supernovae explosions, acting as standard candles, lead to different predictions in an inhomogeneous universe, which are disfavored by current data. The conclusion of the analysis is that the use of purely geometric probes, that only recently have become sufficiently constraining, is able to rule out the whole class of adiabatic LTB models. This is independent of other dynamical constraints, like those coming from the kinematic Sunyaev-Zel'dovich effect or the integrated Sachs-Wolfe effect, which in the near future can be used to definitely rule out all inhomogeneous models without dark energy. The present results are also relevant for observationally constraining more general inhomogeneous models [103] including some recent proposals that also include dark energy [104–107].

Acknowledgments

We thank Troels Haugbolle, David Alonso, Savvas Nesseris, Domenico Sapone, Eusebio Sanchez, Enrique Gaztañaga and Alicia Bueno Beloso for enlightening discussions at various stages of the paper, as well as Sean February, Seshadri Nadathur and James Zibin for correspondence and comments to the first version. We also acknowledge financial support from the Madrid Regional Government (CAM) under the program HEPHACOS S2009/ESP-1473-02, from MICINN under grant AYA2009-13936-C06-06 and Consolider-Ingenio 2010 PAU (CSD2007-00060), as well as from the European Union Marie Curie Initial Training Network "UNILHC" PITN-GA-2009-237920. MZ is supported by MICINN (Spain) through the project AYA2006-05369 and the grant BES-2008-009090, and enjoyed an Yggdrasil grant from the Norwegian Research Council while completing this project.

References

- [1] **Supernova Cosmology Project** Collaboration, S. Perlmutter *et. al.*, *Measurements of Omega and Lambda from 42 high redshift supernovae*, *Astrophys.J.* **517** (1999) 565–586, [[astro-ph/9812133](#)].
- [2] **Supernova Search Team** Collaboration, A. G. Riess *et. al.*, *Observational evidence from supernovae for an accelerating universe and a cosmological constant*, *Astron.J.* **116** (1998) 1009–1038, [[astro-ph/9805201](#)].
- [3] N. Mustapha, C. Hellaby, and G. Ellis, *Large scale inhomogeneity versus source evolution: Can we distinguish them observationally?*, *Mon.Not.Roy.Astron.Soc.* **292** (1997) 817–830, [[gr-qc/9808079](#)].
- [4] M.-N. Celerier, *Do we really see a cosmological constant in the supernovae data?*, *Astron.Astrophys.* **353** (2000) 63–71, [[astro-ph/9907206](#)].
- [5] K. Tomita, *A local void and the accelerating universe*, *Mon.Not.Roy.Astron.Soc.* **326** (2001) 287, [[astro-ph/0011484](#)].
- [6] H. Alnes, M. Amarsguioi, and O. Gron, *An inhomogeneous alternative to dark energy?*, *Phys.Rev.* **D73** (2006) 083519, [[astro-ph/0512006](#)].
- [7] R. A. Vanderveld, E. E. Flanagan, and I. Wasserman, *Mimicking dark energy with Lemaitre-Tolman-Bondi models: Weak central singularities and critical points*, *Phys.Rev.* **D74** (2006) 023506, [[astro-ph/0602476](#)].
- [8] D. Garfinkle, *Inhomogeneous spacetimes as a dark energy model*, *Class.Quant.Grav.* **23** (2006) 4811–4818, [[gr-qc/0605088](#)].
- [9] K. Enqvist, *Lemaitre-Tolman-Bondi model and accelerating expansion*, *Gen.Rel.Grav.* **40** (2008) 451–466, [[arXiv:0709.2044](#)].

- [10] T. Mattsson, *Dark energy as a mirage*, *Gen.Rel.Grav.* **42** (2010) 567–599, [[arXiv:0711.4264](#)].
- [11] S. Sarkar, *Is the evidence for dark energy secure?*, *Gen.Rel.Grav.* **40** (2008) 269–284, [[arXiv:0710.5307](#)].
- [12] J. Zibin, A. Moss, and D. Scott, *Can we avoid dark energy?*, *Phys.Rev.Lett.* **101** (2008) 251303, [[arXiv:0809.3761](#)].
- [13] T. Clifton, P. G. Ferreira, and K. Land, *Living in a Void: Testing the Copernican Principle with Distant Supernovae*, *Phys.Rev.Lett.* **101** (2008) 131302, [[arXiv:0807.1443](#)].
- [14] J. Moffat, *Void or Dark Energy?*, [[arXiv:0910.2723](#)].
- [15] M.-N. Celerier, K. Bolejko, and A. Krasinski, *A (giant) void is not mandatory to explain away dark energy with a Lemaitre – Tolman model*, *Astron.Astrophys.* **518** (2010) A21, [[arXiv:0906.0905](#)].
- [16] R. A. Vanderveld, E. E. Flanagan, and I. Wasserman, *Lemaitre-Tolman-Bondi cosmological models, smoothness, and positivity of the central deceleration parameter*, [[arXiv:0904.4319](#)].
- [17] M. Regis and C. Clarkson, *Do primordial Lithium abundances imply there’s no Dark Energy?*, [[arXiv:1003.1043](#)].
- [18] T. Buchert, *Toward physical cosmology: focus on inhomogeneous geometry and its non-perturbative effects*, [[arXiv:1103.2016](#)].
- [19] G. F. Ellis, *Inhomogeneity effects in Cosmology*, [[arXiv:1103.2335](#)].
- [20] T. Buchert and S. Rasanen, *Backreaction in late-time cosmology*, [[arXiv:1112.5335](#)].
- [21] K. Enqvist and T. Mattsson, *The effect of inhomogeneous expansion on the supernova observations*, *JCAP* **0702** (2007) 019, [[astro-ph/0609120](#)].
- [22] S. Alexander, T. Biswas, A. Notari, and D. Vaid, *Local Void vs Dark Energy: Confrontation with WMAP and Type Ia Supernovae*, *JCAP* **0909** (2009) 025, [[arXiv:0712.0370](#)].
- [23] J. Garcia-Bellido and T. Haugboelle, *Confronting Lemaitre-Tolman-Bondi models with Observational Cosmology*, *JCAP* **0804** (2008) 003, [[arXiv:0802.1523](#)].
- [24] J. Garcia-Bellido and T. Haugboelle, *The radial BAO scale and Cosmic Shear, a new observable for Inhomogeneous Cosmologies*, *JCAP* **0909** (2009) 028, [[arXiv:0810.4939](#)].
- [25] A. E. Romano, *Mimicking the cosmological constant for more than one observable with large scale inhomogeneities*, *Phys.Rev.* **D82** (2010) 123528, [[arXiv:0912.4108](#)].
- [26] S. February, J. Larena, M. Smith, and C. Clarkson, *Rendering Dark Energy Void*, *Mon.Not.Roy.Astron.Soc.* **405** (2010) 2231, [[arXiv:0909.1479](#)].
- [27] M. Quartin and L. Amendola, *Distinguishing Between Void Models and Dark Energy with Cosmic Parallax and Redshift Drift*, *Phys.Rev.* **D81** (2010) 043522, [[arXiv:0909.4954](#)].
- [28] A. Moss, J. P. Zibin, and D. Scott, *Precision Cosmology Defeats Void Models for Acceleration*, *Phys.Rev.* **D83** (2011) 103515, [[arXiv:1007.3725](#)].
- [29] T. Biswas, A. Notari, and W. Valkenburg, *Testing the Void against Cosmological data: fitting CMB, BAO, SN and H_0* , *JCAP* **1011** (2010) 030, [[arXiv:1007.3065](#)].
- [30] P. Dunsby, N. Goheer, B. Osano, and J.-P. Uzan, *How close can an Inhomogeneous Universe mimic the Concordance Model?*, *JCAP* **1006** (2010) 017, [[arXiv:1002.2397](#)].
- [31] S. Nadathur and S. Sarkar, *Reconciling the local void with the CMB*, *Phys.Rev.* **D83** (2011) 063506, [[arXiv:1012.3460](#)].
- [32] V. Marra and M. Paakkonen, *Observational constraints on the LLTB model*, *JCAP* **1012** (2010) 021, [[arXiv:1009.4193](#)].
- [33] P. Zhang and A. Stebbins, *Confirmation of the Copernican principle at Gpc radial scale and*

- above from the kinetic Sunyaev Zel'dovich effect power spectrum, *Phys.Rev.Lett.* **107** (2011) 041301, [[arXiv:1009.3967](#)].
- [34] C.-M. Yoo, T. Kai, and K.-i. Nakao, *Redshift Drift in LTB Void Universes*, *Phys.Rev.* **D83** (2011) 043527, [[arXiv:1010.0091](#)].
- [35] V. Marra and A. Notari, *Observational constraints on inhomogeneous cosmological models without dark energy*, *Class.Quant.Grav.* **28** (2011) 164004, [[arXiv:1102.1015](#)].
- [36] P. Bull, T. Clifton, and P. G. Ferreira, *The kSZ effect as a test of general radial inhomogeneity in LTB cosmology*, [arXiv:1108.2222](#).
- [37] A. E. Romano, *Do recent accurate measurements of H_0 really rule out void models as alternatives to dark energy?*, [arXiv:1105.1864](#).
- [38] H. Wang and T.-J. Zhang, *Constraints on Lemaitre-Tolman-Bondi models from Observational Hubble Parameter data*, [arXiv:1111.2400](#).
- [39] J. P. Zibin, *Scalar Perturbations on Lemaitre-Tolman-Bondi Spacetimes*, *Phys.Rev.* **D78** (2008) 043504, [[arXiv:0804.1787](#)].
- [40] C. Clarkson, T. Clifton, and S. February, *Perturbation Theory in Lemaitre-Tolman-Bondi Cosmology*, *JCAP* **0906** (2009) 025, [[arXiv:0903.5040](#)].
- [41] D. Alonso, J. Garcia-Bellido, T. Haugbolle, and J. Vicente, *Large scale structure simulations of inhomogeneous LTB void models*, *Phys.Rev.* **D82** (2010) 123530, [[arXiv:1010.3453](#)].
- [42] R. Nishikawa, C.-M. Yoo, and K.-i. Nakao, *Evolution of density perturbations in large void universe*, [arXiv:1202.1582](#).
- [43] D. Alonso, J. Garcia-Bellido, T. Haugboelle, and A. Knebe, *Halo abundances and shear in void models*, [arXiv:1204.3532](#).
- [44] S. February, C. Clarkson, and R. Maartens, *Galaxy correlations and the BAO in a void universe: structure formation as a test of the Copernican Principle*, [arXiv:1206.1602](#).
- [45] J. W. Moffat, *Cosmic microwave background, accelerating Universe and inhomogeneous cosmology*, *JCAP* **0510** (2005) 012, [[astro-ph/0502110](#)].
- [46] H. Alnes and M. Amarzguoui, *CMB anisotropies seen by an off-center observer in a spherically symmetric inhomogeneous Universe*, *Phys.Rev.* **D74** (2006) 103520, [[astro-ph/0607334](#)].
- [47] R. Caldwell and A. Stebbins, *A Test of the Copernican Principle*, *Phys.Rev.Lett.* **100** (2008) 191302, [[arXiv:0711.3459](#)].
- [48] J. Garcia-Bellido and T. Haugboelle, *Looking the void in the eyes - the kSZ effect in LTB models*, *JCAP* **0809** (2008) 016, [[arXiv:0807.1326](#)].
- [49] T. Clifton, P. G. Ferreira, and J. Zuntz, *What the small angle CMB really tells us about the curvature of the Universe*, *JCAP* **0907** (2009) 029, [[arXiv:0902.1313](#)].
- [50] C.-M. Yoo, K.-i. Nakao, and M. Sasaki, *CMB observations in LTB universes: Part I: Matching peak positions in the CMB spectrum*, *JCAP* **1007** (2010) 012, [[arXiv:1005.0048](#)].
- [51] C.-M. Yoo, K.-i. Nakao, and M. Sasaki, *CMB observations in LTB universes: Part II – the kSZ effect in an LTB universe*, *JCAP* **1010** (2010) 011, [[arXiv:1008.0469](#)].
- [52] C. Clarkson and M. Regis, *The Cosmic Microwave Background in an Inhomogeneous Universe - why void models of dark energy are only weakly constrained by the CMB*, *JCAP* **1102** (2011) 013, [[arXiv:1007.3443](#)].
- [53] J. P. Zibin and A. Moss, *Linear kinetic Sunyaev-Zel'dovich effect and void models for acceleration*, *Class.Quant.Grav.* **28** (2011) 164005, [[arXiv:1105.0909](#)].

- [54] J. P. Zibin, *Can decaying modes save void models for acceleration?*, *Phys.Rev.* **D84** (2011) 123508, [[arXiv:1108.3068](#)].
- [55] T. Clifton, C. Clarkson, and P. Bull, *The isotropic blackbody CMB as evidence for a homogeneous universe*, [arXiv:1111.3794](#).
- [56] C. Clarkson, *Establishing homogeneity of the universe in the shadow of dark energy*, [arXiv:1204.5505](#).
- [57] A. D. Linde, D. A. Linde, and A. Mezhlumian, *Do we live in the center of the world?*, *Phys.Lett.* **B345** (1995) 203–210, [[hep-th/9411111](#)].
- [58] A. G. Riess, L. Macri, S. Casertano, H. Lampeitl, H. C. Ferguson, *et. al.*, *A 3% Solution: Determination of the Hubble Constant with the Hubble Space Telescope and Wide Field Camera 3*, *Astrophys.J.* **730** (2011) 119, [[arXiv:1103.2976](#)].
- [59] C. Blake, E. Kazin, F. Beutler, T. Davis, D. Parkinson, *et. al.*, *The WiggleZ Dark Energy Survey: mapping the distance-redshift relation with baryon acoustic oscillations*, [arXiv:1108.2635](#).
- [60] A. Carnero, E. Sanchez, M. Crocce, A. Cabre, and E. Gaztanaga, *Clustering of Photometric Luminous Red Galaxies II: Cosmological Implications from the Baryon Acoustic Scale*, *Monthly Notices of the Royal Astronomical Society* **Volume 419, Issue 2** (2011) 16891694, [[arXiv:1104.5426](#)].
- [61] G. Lemaitre, *The expanding universe*, *Gen.Rel.Grav.* **29** (1997) 641–680.
- [62] R. C. Tolman, *Effect of inhomogeneity on cosmological models*, *Proc.Nat.Acad.Sci.* **20** (1934) 169–176.
- [63] H. Bondi, *Spherically symmetrical models in general relativity*, *Mon.Not.Roy.Astron.Soc.* **107** (1947) 410–425.
- [64] D. J. Eisenstein and W. Hu, *Baryonic features in the matter transfer function*, *Astrophys.J.* **496** (1998) 605, [[astro-ph/9709112](#)].
- [65] **SDSS Collaboration** Collaboration, D. J. Eisenstein *et. al.*, *Detection of the baryon acoustic peak in the large-scale correlation function of SDSS luminous red galaxies*, *Astrophys.J.* **633** (2005) 560–574, [[astro-ph/0501171](#)].
- [66] S. Dodelson, *Modern cosmology*. Academic Pr., 2003.
- [67] M. Crocce and R. Scoccimarro, *Nonlinear Evolution of Baryon Acoustic Oscillations*, *Phys.Rev.* **D77** (2008) 023533, [[arXiv:0704.2783](#)].
- [68] R. E. Smith, R. Scoccimarro, and R. K. Sheth, *Eppur Si Muove: On The Motion of the Acoustic Peak in the Correlation Function*, *Phys.Rev.* **D77** (2008) 043525, [[astro-ph/0703620](#)].
- [69] B. A. Bassett and R. Hlozek, *Baryon Acoustic Oscillations*, [arXiv:0910.5224](#).
- [70] C. Alcock and B. Paczynski, *An evolution free test for non-zero cosmological constant*, *Nature* **281** (1979) 358–359.
- [71] C. Blake, K. Glazebrook, T. Davis, S. Brough, M. Colless, *et. al.*, *The WiggleZ Dark Energy Survey: measuring the cosmic expansion history using the Alcock-Paczynski test and distant supernovae*, [arXiv:1108.2637](#).
- [72] E. A. Kazin, A. G. Sanchez, and M. R. Blanton, *Improving measurements of $H(z)$ and $D_A(z)$ by analyzing clustering anisotropies*, *Mon.Not.Roy.Astron.Soc.* **419** (2012) 3223–3243, [[arXiv:1105.2037](#)].
- [73] X. Xu, A. J. Cuesta, N. Padmanabhan, D. J. Eisenstein, and C. K. McBride, *Measuring D_A and H at $z = 0.35$ from the SDSS DR7 LRGs using baryon acoustic oscillations*,

[arXiv:1206.6732](#).

- [74] R. Amanullah, C. Lidman, D. Rubin, G. Aldering, P. Astier, *et. al.*, *Spectra and Light Curves of Six Type Ia Supernovae at $0.511 < z < 1.12$ and the Union2 Compilation*, *Astrophys.J.* **716** (2010) 712–738, [[arXiv:1004.1711](#)].
- [75] **Supernova Cosmology Project** Collaboration, M. Kowalski *et. al.*, *Improved Cosmological Constraints from New, Old and Combined Supernova Datasets*, *Astrophys.J.* **686** (2008) 749–778, [[arXiv:0804.4142](#)].
- [76] B. A. Reid, W. J. Percival, D. J. Eisenstein, L. Verde, D. N. Spergel, *et. al.*, *Cosmological Constraints from the Clustering of the Sloan Digital Sky Survey DR7 Luminous Red Galaxies*, *Mon.Not.Roy.Astron.Soc.* **404** (2010) 60–85, [[arXiv:0907.1659](#)].
- [77] **SDSS Collaboration** Collaboration, W. J. Percival *et. al.*, *Baryon Acoustic Oscillations in the Sloan Digital Sky Survey Data Release 7 Galaxy Sample*, *Mon.Not.Roy.Astron.Soc.* **401** (2010) 2148–2168, [[arXiv:0907.1660](#)].
- [78] F. Beutler, C. Blake, M. Colless, D. H. Jones, L. Staveley-Smith, *et. al.*, *The 6dF Galaxy Survey: Baryon Acoustic Oscillations and the Local Hubble Constant*, *Mon.Not.Roy.Astron.Soc.* **416** (2011) 3017–3032, [[arXiv:1106.3366](#)].
- [79] A. G. Sanchez, C. M. Baugh, and R. Angulo, *What is the best way to measure baryonic acoustic oscillations?*, *Mon.Not.Roy.Astron.Soc.* **390** (2008) 1470–1490, [[arXiv:0804.0233](#)].
- [80] **SDSS Collaboration** Collaboration, E. A. Kazin *et. al.*, *The Baryonic Acoustic Feature and Large-Scale Clustering in the SDSS LRG Sample*, *Astrophys.J.* **710** (2010) 1444–1461, [[arXiv:0908.2598](#)].
- [81] K. T. Mehta, A. J. Cuesta, X. Xu, D. J. Eisenstein, and N. Padmanabhan, *A 2% Distance to $z = 0.35$ by Reconstructing Baryon Acoustic Oscillations - III : Cosmological Measurements and Interpretation*, [arXiv:1202.0092](#).
- [82] L. Anderson, E. Aubourg, S. Bailey, D. Bizyaev, M. Blanton, *et. al.*, *The clustering of galaxies in the SDSS-III Baryon Oscillation Spectroscopic Survey: Baryon Acoustic Oscillations in the Data Release 9 Spectroscopic Galaxy Sample*, [arXiv:1203.6594](#).
- [83] E. Gaztanaga, A. Cabre, and L. Hui, *Clustering of Luminous Red Galaxies IV: Baryon Acoustic Peak in the Line-of-Sight Direction and a Direct Measurement of $H(z)$* , *Mon.Not.Roy.Astron.Soc.* **399** (2009) 1663–1680, [[arXiv:0807.3551](#)].
- [84] E. Gaztanaga, R. Miquel, and E. Sanchez, *First Cosmological Constraints on Dark Energy from the Radial Baryon Acoustic Scale*, *Phys.Rev.Lett.* **103** (2009) 091302, [[arXiv:0808.1921](#)].
- [85] **WMAP Collaboration** Collaboration, E. Komatsu *et. al.*, *Seven-Year Wilkinson Microwave Anisotropy Probe (WMAP) Observations: Cosmological Interpretation*, *Astrophys.J.Suppl.* **192** (2011) 18, [[arXiv:1001.4538](#)].
- [86] M. Vonlanthen, S. Rasanen, and R. Durrer, *Model-independent cosmological constraints from the CMB*, *JCAP* **1008** (2010) 023, [[arXiv:1003.0810](#)].
- [87] P. D. Lasky and K. Bolejko, *The effect of pressure gradients on luminosity distance - redshift relations*, *Class.Quant.Grav.* **27** (2010) 035011, [[arXiv:1001.1159](#)].
- [88] V. Marra and M. Paakkonen, *Exact spherically-symmetric inhomogeneous model with n perfect fluids*, *JCAP* **1201** (2012) 025, [[arXiv:1105.6099](#)].
- [89] D. Larson, J. Dunkley, G. Hinshaw, E. Komatsu, M. Nolta, *et. al.*, *Seven-Year Wilkinson Microwave Anisotropy Probe (WMAP) Observations: Power Spectra and WMAP-Derived Parameters*, *Astrophys.J.Suppl.* **192** (2011) 16, [[arXiv:1001.4635](#)].
- [90] W. Hu and N. Sugiyama, *Small scale cosmological perturbations: An Analytic approach*,

- Astrophys.J.* **471** (1996) 542–570, [[astro-ph/9510117](#)].
- [91] M. Doran and M. Lilley, *The Location of CMB peaks in a universe with dark energy*, *Mon.Not.Roy.Astron.Soc.* **330** (2002) 965–970, [[astro-ph/0104486](#)].
- [92] W. Hu, M. Fukugita, M. Zaldarriaga, and M. Tegmark, *CMB observables and their cosmological implications*, *Astrophys.J.* **549** (2001) 669, [[astro-ph/0006436](#)].
- [93] M. Doran, *Cmbeasy:: an object oriented code for the cosmic microwave background*, *JCAP* **0510** (2005) 011, [[astro-ph/0302138](#)].
- [94] A. Gelman and D. B. Rubin, *Inference from Iterative Simulation Using Multiple Sequences*, *Statist. Sci.* **7** (1992) 457–472.
- [95] M. Doran and C. M. Mueller, *Analyze This! A Cosmological constraint package for CMBEASY*, *JCAP* **0409** (2004) 003, [[astro-ph/0311311](#)].
- [96] L. M. Krauss and B. Chaboyer, *Age Estimates of Globular Clusters in the Milky Way: Constraints on Cosmology*, *Science* **299** (2003) 65–70.
- [97] H. Akaike, *A new look at the statistical model identification*, *IEEE Transactions on Automatic Control* **16** (6):**716–723** (1974).
- [98] G. Schwarz., *Estimating the dimension of a model*, *Annals of Statistics* **6** (2):**461–464** (1978).
- [99] C. Clarkson, B. Bassett, and T. H.-C. Lu, *A general test of the Copernican Principle*, *Phys.Rev.Lett.* **101** (2008) 011301, [[arXiv:0712.3457](#)].
- [100] S. Nesseris and J. Garcia-Bellido, *A new perspective on Dark Energy modeling via Genetic Algorithms*, [arXiv:1205.0364](#).
- [101] L. Amendola, S. Appleby, D. Bacon, T. Baker, M. Baldi, *et. al.*, *Cosmology and fundamental physics with the Euclid satellite*, [arXiv:1206.1225](#).
- [102] M. Beltran, J. Garcia-Bellido, J. Lesgourgues, A. R. Liddle, and A. Slosar, *Bayesian model selection and isocurvature perturbations*, *Phys.Rev.* **D71** (2005) 063532, [[astro-ph/0501477](#)].
- [103] K. Bolejko, M.-N. Celerier, and A. Krasinski, *Inhomogeneous cosmological models: Exact solutions and their applications*, *Class.Quant.Grav.* **28** (2011) 164002, [[arXiv:1102.1449](#)].
- [104] J. Grande and L. Perivolaropoulos, *Generalized LTB model with Inhomogeneous Isotropic Dark Energy: Observational Constraints*, *Phys.Rev.* **D84** (2011) 023514, [[arXiv:1103.4143](#)].
- [105] J. C. Bueno Sanchez and L. Perivolaropoulos, *Topological Quintessence*, *Phys.Rev.* **D84** (2011) 123516, [[arXiv:1110.2587](#)].
- [106] M. Roos, *Quintessence-like Dark Energy in a Lemaître-Tolman-Bondi Metric*, [arXiv:1107.3028](#).
- [107] V. Marra, M. Paakkonen, and W. Valkenburg, *Bias on w from large-scale structure*, [arXiv:1203.2180](#).